PRODUCTION OF SILICA FUME-BASED GEOPOLYMERIC FOAM

A THESIS SUBMITTED TO
THE GRADUATE SCHOOL OF NATURAL AND APPLIED SCIENCES
OF
MIDDLE EAST TECHNICAL UNIVERSITY

BY

SAHRA SHAKOURI

IN PARTIAL FULFILLMENT OF THE REQUIREMENTS
FOR
THE DEGREE OF MASTER OF SCIENCE
IN
CIVIL ENGINEERING

SEPTEMBER 2017

Approval of the thesis:

PRODUCTION OF SILICA FUME BASED GEOPOLYMERIC FOAM

submitted by **SAHRA SHAKOURI** in partial fulfillment of the requirements for the degree of **Master of Science in Civil Engineering Department**, **Middle East Technical University** by,

Prof. Dr. Gülbin Dural Ünvar
Dean, Graduate School of **Natural and Applied Sciences** _____

Prof. Dr. İsmail Özgür Yaman
Head of Department, **Civil Engineering** _____

Assoc. Prof. Dr. Sinan Turhan Erdoğan
Supervisor, **Civil Engineering Dept., METU** _____

Examining Committee Members:

Prof. Dr. Mustafa Tokyay
Civil Engineering Dept., METU _____

Assoc. Prof. Dr. Sinan Turhan Erdoğan
Civil Engineering Dept., METU _____

Assoc. Prof. Dr. Berna Unutmaz
Civil Engineering Dept., Hacettepe University _____

Asst. Prof. Dr. Seda Yeşilmen
Civil Engineering Dept., Çankaya University _____

Asst. Prof. Dr. Çağla Meral
Civil Engineering Dept., METU _____

Date: 04/09/2017

I hereby declare that all information in this document has been obtained and presented in accordance with academic rules and ethical conduct. I also declare that, as required by these rules and conduct, I have fully cited and referenced all material and results that are not original to this work.

Name, Last Name: Sahra Shakouri

Signature:

ABSTRACT

PRODUCTION OF SILICA FUME-BASED GEOPOLYMERIC FOAM

Shakouri, Sahra

M. S., Department of Civil Engineering

Supervisor: Sinan Turhan Erdoğan

September 2017, 81 Pages

This study investigates the activation of silica fume powder with sodium hydroxide solutions, to produce foamy geopolymeric material. The powder was mixed with NaOH solutions of different concentration, at different solution-to-powder ratios and cured at 100 °C for different length of time. Upon to heating to 200-500 °C, a volume expansion up to 10 times of the initial paste volume took palace, and a porous structure resulted. Ground perlite, expanded perlite and basalt fibers were tested as additives to the initial mixtures. The main goal of this study was to reach a uniform foamy structure with as low density as possible. The final density of materials decreased to as low as ~50 kg/m^3. The morphological characteristics of samples were investigated by SEM analyses performed on heat treated products. Compressive strength of expanded materials ranges between 50 kPa and 1 MPa. Also the structural evolution of pastes was determined using FTIR spectroscopy and ^{29}Si MAS NMR measurements. Pore size distribution and pore volumes measured by nitrogen adsorption and x-ray microcomputed tomography.

Keywords: Silica fume, alkali activation, geopolymer, low density, sodium hydroxide, porous foam

ÖZ

SİLİS DUMANI İLE JEOPOLİMERİK KÖPÜK ÜRETİMİ

Shakouri, Sahra
Yüksek Lisans, İnşaat Mühendisliği Bölümü
Tez Yöneticisi: Doç. Dr. Sinan Turhan Erdoğan

Eylül 2017, 81 sayfa

Bu çalışma silis dumanının köpük jeopolimerik malzeme üretimi için sodyum hidroksit çözeltileri ile aktivasyonunu incelemektedir. Toz çeşitli konsantrasyonlarda NaOH çözeltisi ile, farklı çözelti-tozu oranlarında karıştırılmış ve 100 °C 'de farklı süreler boyunca kürlenmiştir. 200-500 °C 'de ısıtılması ile, ilk hamurun 10 katına kadar varan hacim artışları gözlenmiş ve gözenekli bir yapı ortaya çıkmıştır. İlk hamur karışımına öğütülmüş perlit, genleşmiş perlit, ve bazalt liflerinin katkı olarak eklenmesi de denenmiştir. Bu çalışmanın ana hedefi mümkün olan en düşük yoğunluğa sahip homojen köpük yapının elde edilmesidir. Üretilen malzemelerin son yoğunluğu ~50 kg /m^3 'e kadar düşürülebilmektedir. Numunelerin morfolojik özellikleri SEM analizi ile incelenmiştir. Genleşmiş malzemelerin basınç dayanımları 50 kPa ile 1 MPa aralığında ölçülmüştür. Hamurların yapısal değişimi de FTIR spektroskopisi ve ^{29}Si MAS NMR ile belirlenmiştir. Gözenek boy dağılımı ve gözenek hacmi, azot adsorpsiyonu ile ve x-ışını mikrotomografı yöntemleriyle ölçülmüştür.

Anahtar Kelimeler: Silika dumanı, alkali aktivasyon, jeopolimer, düşük yoğunluk, sodyum hidroksit, gözenekli köpük.

To my Beloved Family

ACKNOWLEDGMENTS

TABLE OF CONTENTS

LIST OF TABLES

TABLES

LIST OF FIGURES

FIGURES

CHAPTER 1

INTRODUCTION

1.1   Background

Research about energy consumption in 27 members of European Union in households and services sector shows a continuous increase during the past 15 years, from 388.5 Mtoe in 1990 to 434.0 Mtoe in 2014 (EU energy and transport, 2014). A high portion of this increase is related to building heating and air conditioning. To reverse this increasing trend of energy consumption, the EU has made the use of thermal insulation mandatory in most European countries and the development of new and effective insulators has become an important and progressing field (Papadopoulos, 2005; Vaou & Panias, 2010).

Insulating materials can be divided into several subgroups according to their physical and chemical structures. The two main groups are organic and inorganic materials. Organic materials contain expanded polystyrene, extruded polystyrene, polyurethane foam etc. All of which have their own problems. For example, polystyrene products are very flammable and also after ignition produce polycyclic aromatic hydrocarbons which are dangerous for human health and also the decomposition period for this material is very long which is a disadvantage from an environmental point of view. Another problem is polystyrene products become brittle under direct sunlight exposure (Papadopoulos, 2005).

Fibrous glass and stone wools are the most common inorganic insulators used in the EU market. Despite being resistant to fire and high temperatures, these fibers can cause skin irritation and respiratory problems.

Another group of inorganic insulating materials composes silicon or carbon aerogels which have the best insulating performance ever reported and extremely low density. The bulk density of these aerogels is <150 kg/m^3 and can be as low as 3 kg/m^3 (Dorcheh & Abbasi, 2008). The main problems with this material are its high cost, which limits its usage just in special applications and that they could not be produced in large volumes due to processing requirements (Sadineni et al., 2011; Dorcheh & Abbasi, 2008).

These disadvantages of common insulating materials have motivated the researchers to seek more economical and practical replacements. Alkali-activated materials are one such alternative for making new intumescent and porous materials (Erdoğan, 2015).

The very first idea about the reaction of alkali sources and alumina-silica rich solids to produce a material properties similar to hardened concrete, was noted in 1900s. These new materials were performed in the 1940s by studies on using blast furnace slag and sodium hydroxide solutions with various other additives. In 1970s, Davidovits proposed that these systems could be used to produce fire-resistant materials (Davidovits, 2008; Provis & van Deventer, 2013). One of the reasons for the popularity of these new materials among researchers is that they can employ transforming by-products or low-value materials like fly ash, blast furnace slag as the aluminosilicate powder, providing economical and environmental advantages.

1.2 Objective and Scope

In this thesis, the production of a new alkali-activated material made by activating silica fume (of high silica content) with an economical alkali compound (NaOH) is studied, with the goal of obtaining a lightweight (density lower than 100 kg/m^3) and intumescent (able to expand upon exposure to heat) material. Methods of production and some properties of this foam material are investigated.

In Chapter two, a brief description of porous materials, alkali activated materials and their history, and related properties is given, along with a brief introduction of silica

fume. Chapter three includes information about all the raw materials used in the experiments, and also describes the mixing and production procedures, and briefly introduced the test methods used. Chapter four provides the results of the different tests conducted and Chapter five lists the conclusions of this study and provides some suggestions and recommendations for future studies.

CHAPTER 2

LITERATURE REVIEW

2.1 Porous Materials

Almost all the materials around us are a little bit porous (Rouquerol et al., 1994). Porous materials can be defined as materials consisting of a rigid solid part (solid phase) that makes up the structural section of material and a void network (fluid phase) that makes up the pores inside the solid. In addition, porous materials have two other characteristics: 1) multiple pores should exist inside the materials, not just one or two pores like cavities, 2) pores inside the materials should improve specific properties, not to reduce the quality of materials (Aït-Mokhtar et al., 2015; Liu and Chen, 2014). One of the most important factors specified in porous materials is porosity, defined as the ratio of pore volume to the total volume of the object. Porosity influences the physical properties of the medium like density, strength, and conductivity, and also the chemical reactivity (Rouquerol et al., 1994).

2.1.1 Categorization of Porous Materials

Porous materials can be grouped according to different criteria, which are given in the following sections.

2.1.1.1 Source of Materials

Like most other materials, porous materials can have two origins, natural or artificial. Natural porous materials exist all over the world as bones, leaves, and trunks of the trees (most of the time the fluid phase of materials in this group is liquid), pumice, coral, lava, etc. Artificial porous materials can be divided into three subgroups as porous metals, porous ceramics, and polymer foams. Unlike natural porous materials, the fluid phase of these groups is often a gas (Liu and Chen, 2014).

2.1.1.2 Shape and Size of Pores

One of the most important features in porous material is pore size, to the extent that materials with similar porosity and different pore sizes have differently reactions in the same conditions. Pore size is important especially when pore shape is determined (Zdravkov et al., 2007).

Different ideas exist about the geometry of pores. Similar materials generally have similar pore shapes. They can be classified as spherical pores such as those that appear in gels, plate-like pores in clay and activated carbon, cylindrical pores exist in activated oxides like alumina or magnesia, prismatic as in fibrous zeolites, ink bottle, cone-shaped or funnel-shaped (Zdravkov et al., 2007).

The International Union of Pure and Applied Chemistry (IUPAC) classifies materials in three groups according to pore size (Ishizaki et al., 2013; Rouquerol et al., 1994):

- Microporous materials: pore diameter smaller than 2 *nm*
- Mesoporous materials: pore diameter between 2 *nm* and 50 *nm*
- Macroporous materials: pore diameter larger than 50 *nm*

Microporous materials have further been categorized into three subgroups from small to large respectively: sub-microporous, ultra-microporous and super-microporous materials (Zdravkov et al., 2007).

2.1.1.3 Accessibility of Pores

Pores can be also categorized according to their accessibility to their surroundings or according to the ability of an external liquid to penetrate inside the body.

Pores labeled (a) in Figure 2.1 are named isolated pores. This kind of pore has an important role in determining physical properties like compressive strength, bulk density, and thermal conductivity. They form when the porous solid is heated insufficiently or when the production of a gaseous substance inside the particle is not enough (Rouquerol et al., 1994).
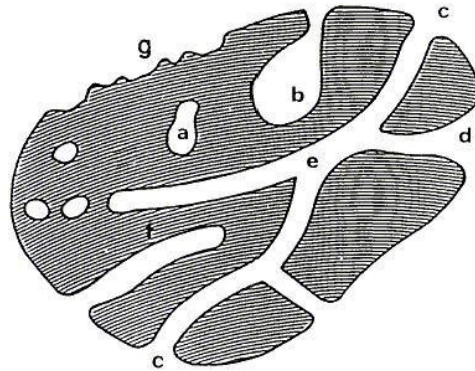
Figure 2.1 Pore types according to accessibility (Rouquerol et al., 1994)

All the pores except (a) are open pores because they have access to the surface of the solid, and ions and molecules can penetrate the solid through. These open pores also have different types: Pores labeled (b) have ink bottle shape and are also named blind pores because just one end of the pore is open. (c) and (d) are open pores with the cylindrical and funnel shapes respectively. (f) is also a blind pore but it has a cylindrical shape. Some pores like (e) are open at two ends and they are named through pores or penetrating pores. About (g) there is a possible conflict: if the depth of irregularities is more than their width they are considered as pores otherwise they are called roughness (Rouquerol et al., 1994; Zdravkov et al., 2007).

2.2   Silica Fume

2.2.1   Introduction

Silica fume is the byproduct of the manufacturing of silicon metal or ferrosilicon alloys, and before the 1970s it was simply released from the stack of factories to the air, but with changes in the environmental laws, factories began to collect this powder with dust collectors. For manufacturing silica fume, high-purity quartz is smelted in the furnace at 2000 °C and silicon monoxide is produced during the process and oxidized with O_2 in the air, generating SiO_2 (Erdoğan, 1997).

Silica fume is one of the most effective pozzolanic materials meaning it won't react with water individually, but it improves the properties of concrete as it is added to concrete. It happens because of: a) its fineness (specific surface area of silica fume is about 200,000 cm^2/g, ~100 times finer than ordinary Portland cement), b) its spherical shape, c) its high amorphous content (Bapat, 2012).

2.2.2 Forms of Silica Fume

Silica fume is traded in four types:

- **Powder or undensified silica fume**: Bulk density of undensified silica fume can be up to 350 kg/m^3, in comparison to normal Portland cement (~1000−1200 kg/m^3) it has much lower density. Its low bulk density and its dusty and sticky form cause some handling and transportation problems. Undensified silica fume has limited usage in blended cement, grouts and repair mortar.

- **Densified or compacted silica fume:** By densification of undensified silica fume its bulk density increases to ~ 480 to 720 kg/m^3, so some of the previously noted problems are resolved. Densification is done by blowing air from the bottom of the silos in which undensified silica fume is stored. By this method, silica fume particles rub each other and van der Waals force formed on the surface of them causes agglomeration and a higher bulk density. The final particles are similar to small beads and produce less dust.

- **Pelletized Silica Fume:** Undensified silica fume is mixed with water and pelletized in ~10-25-mm diameter discs which are too hard to use directly in concrete and other mixtures. They can be interground with cement clinker to obtain silica fume-blended cement. The bulk density of pelletized silica fume is about 1000 $kg/m^3.$

- **Slurried silica fume:** Another method for countering the problems with undensified silica fume is mixing silica fume with water as 50 - 60 % of the mass. Bulk density in this kind of silica fume increases to ~1300-1400 kg/m^3,

making it more economical to transport and handle. Chemical admixtures like retarders, water reducer, and superplasticizers can also be added to the slurry.

2.2.3 Composition and Chemical Properties of Silica Fume

The high reactivity of silica fume is due to 85-98 % amorphous silica content. Other compounds such as oxides of iron, aluminum, calcium, magnesium, potassium, sulfur, sodium and crystalline forms of silicon are found in very small amounts in silica fume (Bapat, 2012). The general composition of silica fume obtained from different sources is given in Table 2.1.

Table 2.1 Typical composition of SF obtained from different sources(Bapat, 2012)

Constituent	Source and Composition		
	Silicon	Ferrosilicon	Silicon Quarry
SiO_2	97.5	96	92.48
C	0.4	0.5	—
Fe_2O_3	0.03	0.5	0.09
Al_2O_3	0.29	0.20	2.6
CaO	0.20	0.20	0.31
MgO	0.10	0.50	0.0
K_2O^b	0.20	0.50	0.04
Na_2O	0.10	0.20	1.08
Cl	0.01	0.01	—
SO_3	0.10	0.15	0.09
Moisture	0.20	0.50	—
Loss on ignition [$T = 975°C$]	0.70	0.70	1.85

2.2.4 Physical Properties

Silica fume is light to dark in gray color, depending on impurities like carbon and iron oxide. As the amount of impurities increases, the silica fume becomes darker (Chandra & Berntsson, 1996).

2.2.5   Effect of Silica Fume in Concrete

Silica fume can be used in concrete in two ways; first as an additive in concrete and second as a replacement for Portland cement. Because of its chemical and physical properties, silica fume is an effective choice for increasing the performance of concrete. Other mineral and chemical admixtures like fly ash and granulated blast furnace slag can be used in concrete reducing the amount of cement and besides improving the properties of concrete, lessening the cost of concrete, but this aspect is not true for silica fume. Silica fume containing concrete needs more superplasticizer and air entering agents and these factors impact the cost of concrete negatively (Bapat, 2012).

2.3   Alkali-Activated Materials

With increasing global population, the increasing need for civil construction makes concrete the most required substance after water, air pollution results from cement production, consumed in this great amount of concrete. Cement factories emit 4 billion tons of CO_2 each year and this makes up ~6 -7 % of total emitted CO_2 (Van Oss, 2014). The growing need for concrete and the significant air pollution associated with it has led researchers to seek a more environmentally-friend replacement (Shi et al., 2011).

On the other hand, after some catastrophic fires in France in the 1970s, research was begun to develop new fire-resistant materials and "geopolymers" were introduced. Because of using greater amounts of pozzolanic materials than ordinary concrete it is suggested that geopolymers can have a lower impact on the environment. Besides these advantages, other properties like high early compressive strength and low porosity make this kind of alkali-activated materials popular among researchers (Davidovits, 1994; Singh et al., 2015).

Alkali-activated materials are a wide category of man-made substances and are commonly produced from the reaction of a strong alkali, mostly in liquid form and solid aluminosilicates. These aluminosilicates are generally natural pozzolans or other materials which have pozzolanic characteristic when blended with Portland cement

like fly ash, blast furnace slag, metakaolin and rice husk ash (Abdullah et al., 2012; Bernal & Provis, 2014).

During the alkali activation reactions, Si-O-Si bonds in the solids break and Al atoms penetrate to the structure and begin to polymerize. In other words, in corrosive alkaline environments, the aluminosilicates decompose to $[SiO_4]^-$ and $[AlO_4]^-$ and these components polymerize by sharing oxygen atoms and compose a polymer with the general formula $M_n[-(Si-O)_z-Al-O]_n$, where M stands for cations in the alkaline solution like Na, K, and Ca, n is the degree of polycondensations and z could be 1, 2, 3. (Davidovits, 1994; Olvianas et al., 2015; Singh et al., 2015). Equation 2.1 shows the chemical reactions happening during the geopolymerization.

$$(Si_2O_5.Al_2O_2)_n + H_2O + OH^- \rightarrow Si(OH)_4 + Al(OH)^{4-}$$

$$Si(OH)_4 + Al(OH)^{4-} \rightarrow (-Si-O-Al-O-)_n + 4H_2O \qquad \text{(Equation 2-1)}$$
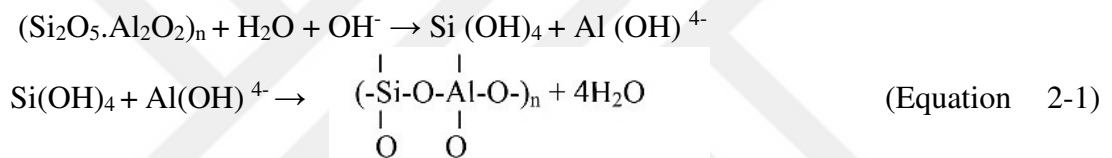
Figure 2.2 shows the steps of alkali-activation schematically, and categorizes this reaction in two groups, for low and high-Ca content aluminosilicates. First, Al^{3+} and Si^{4+} dissolve in the alkaline solution and then these ions reposition in the alkaline medium and finally, the hardening step named poly-condensation begins, which generally produces Al–O–Si polymers. The right side of Figure 2.2 shows the steps for low calcium content and the left side for high calcium content. The differences between these two types are described in the following sections.
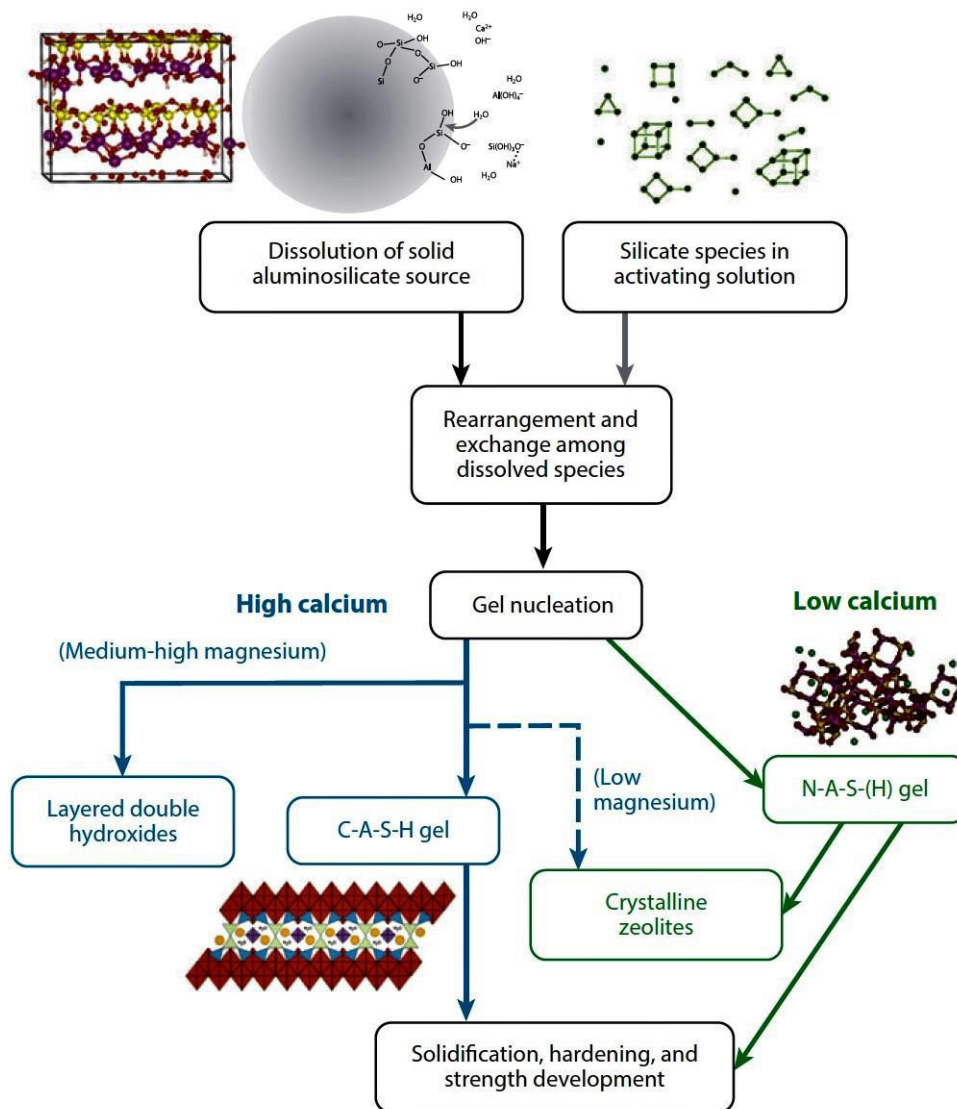
Figure 2.2 Comparison of high and low calcium alkali-activated material (Provis & Bernal, 2014)

There is some disagreement among researchers about the naming and categorization of alkali-activated materials (AAM) and geopolymers. Considering the calcium contents of their precursors and raw materials, AAMs can be categorized into two groups:

2.3.1 High-Calcium Alkali-Activated Materials

Slag is perhaps the most typical high-calcium aluminosilicate powder activated with alkalis. The product of the alkali activation of slag is a CSH gel with the replacement of Si with Al in some cases and it has a disordered tobermorite-like structure. The ratio of Ca/Si mostly depends on the properties of the activator meaning this ratio is higher in NaOH activation in comparison with alkali silicate activation. The CSH gel produced contains layers of silicate chains like in Portland cement hydration. As shown in Figure 2.3 the interlayer part includes different species like cations and hydration water. Also, there is no $Ca(OH)_2$ in the structure of activated blast furnace slag.
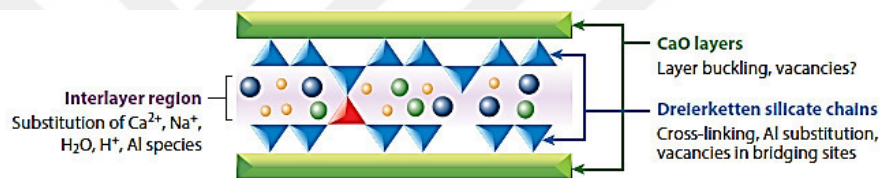
Figure 2.3 Structure of high-calcium alkali-activated materials (Provis & Bernal, 2014)

2.3.2 Low-Calcium Alkali-Activated Materials

Metakaolin and low-calcium (ASTM C150 class F) fly ashes are examples of low-calcium alkali-activated materials. Alkali-activation of these materials creates a material with the general formula of $M_n\{-(SiO_2)_z-AlO\}_n,wH_2O$, where M indicates a cation like Na, Mg, Ca, and n shows the degree of polycondensation, w varies as a function of hydratation of the aluminosilicate. The structure of this group is similar to that of a zeolite. SiO_4 and AlO_4 are connected with oxygen atom bridges and Na or other cations exist to balance the negative charge because of the existence of Al atoms.

13

2.4   Geopolymers

There are two different ideas about geopolymers. Davidovits (1994) considers all alkali activated materials to be geopolymers because all of them have polymeric structures, but Bernal and Provis (2014) argue that alkali-activated materials comprise a wide range of materials and geopolymers are just a low-calcium subgroup of these materials (Provis & van Deventer, 2013). This categorization is shown in Figure 2.4 in order to increasing Ca, Al and alkalinity of solution.
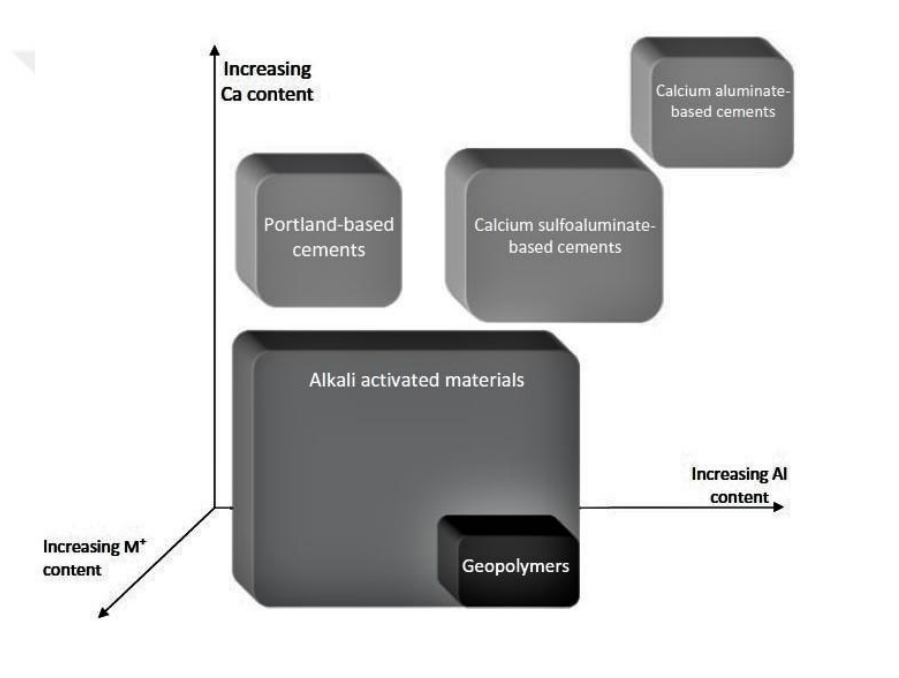
Figure 2.4 Categorization of AAMs and geopolymers (Provis & van Deventer, 2013)

2.5   Lightweight Concretes and Foams

Researchers have long tried to reduce the specific weight of concrete by different methods and for different reasons. One of the most important reasons is that concrete is responsible for half of the dead weight of buildings and a reduction in this weight would improve buildings economically. Another benefit of using lightweight

concretes is their heat insulation property. Air voids are commonly used to reduce the weight of concrete and air is an effective insulator. Considering the manufacturing process and usage, lightweight concretes can be categorized into three groups, are explained briefly in the following sections.

2.5.1 Lightweight Aggregate Concretes

In this type of concrete instead of normal weight aggregate, lightweight aggregate is used and this change reduces the density of concrete from 2400 kg/m^3 to 1850 kg/m^3. Most of the time these lightweight aggregates are natural volcanic aggregates like diatomite, pumice, scoria, etc. or some artificial aggregates like expanded slag and clays. The reason of low density of these aggregates is their porous and vesicular structure. The stiffness of normal aggregates are 4-6 times higher than that of the surrounding mortars and this difference causes stress concentrations under compressive loads, but the stiffness of lightweight concrete is near that of mortar and this stress concentration is omitted (Mindess, 2014; Neville & Brooks, 1987).

2.5.2 Autoclaved Aerated Concrete

Autoclaved aerated concrete (AAC) or gas concrete or cellular concrete is a kind of lightweight concrete made without coarse aggregates. For manufacturing this kind of concrete fine silica sand or Class F fly ash is ground with a ball mill to a specific fineness with cement and water and gas producing agents like metallic aluminum, hydrogen peroxide, and zinc and molded. During the setting of concrete the gas producing agent releases gas bubbles in the mixture and causes expansions (Paillere, 1994). Autoclaving process typically takes 8-12 hours under 12 bar pressure at 180 °C.

$$2Al + 3Ca(OH)_2 + 6H_2O \rightarrow 3CaO.Al_2O_3.6H_2O + 3H_2 \qquad \text{(Equation 2-2)}$$
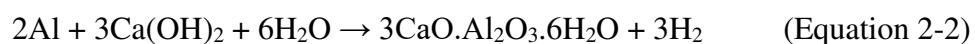
Density limits of AAC concrete are between 350 to 800 kg/m^3 and its compressive strength verifies between 2 and 6 MPa. Most of the time this kind of concrete is used for insulation purposes, fire resistant panels or precast block (Mindess, 2014; Neville & Brooks, 1987).

2.5.3   Foam Concretes

The first foamed concrete was used by Romans about two thousand years ago produced by adding animal blood to the concrete-like mixtures. Nowadays, foam concrete has an ingredient to that in aerated concrete, but instead of a gas-producing agent, a foaming agent is added to the mixture. Foaming agents have two basic types, protein based foaming agents which are made from refined animal products and synthetic surfactants like amines and amine oxides, naphthalene sulphonate formaldehyde condensates. The former group gives higher compressive strength and the latter leads to higher amount of expansion and lower density (Mindess, 2014).

Foams are added to concrete in two states, wet and dry. Spraying a mixture of foaming agent and water from a fine mesh leads to the production of wet foams which makes loose bubbles 2-5 mm in diameter and is not appropriate for making concretes with density lower than 1100 kg/m^3, neither for long distance pumping. Bubbles from a dry foaming agent are about 1 mm in diameter. Dry foam can be blended with the other raw materials to produce a pump able concrete (Ramamurthy et al., 2009). Properties of foam concrete are given in the Table 2.2.

Table 2.2 Typical properties of foam concrete (Limbachiya & Kew, 2008)

Dry density kg/m^3	Compressive strength N/mm^2	Tensile strength N/mm^2	Water Absorption kg/m^2
400	0.5–1.0	.05–0.1	75
600	1.0–1.5	0.2–0.3	33
800	1.5–2.0	0.3–0.4	15
1000	2.5–3.0	0.4–0.6	7
1200	4.5–5.5	0.6–1.1	5
1400	6.0–8.0	0.8–1.2	5
1600	7.5–10.0	1.0–1.6	5

CHAPTER 3

EXPERIMENTS

3.1 Materials and Characterization

Materials which were used in the experiments and their properties are given in this chapter.

3.1.1 Silica Fume

Undensified micro silica, grade 940 from Elkem company was used to produce the samples. It has a dark gray color. Density for this form of silica fume is declared about ~200-350 kg/m^3. Particle size distribution of silica fume measured is displayed in Figure 3.1, also the physical properties of silica fume used in the further experiments are specified in Table 3.1.
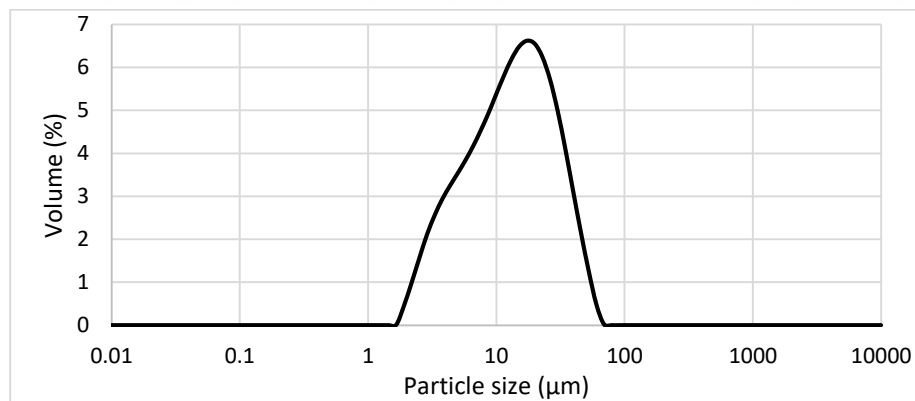
Figure 3.1 Particle size distribution of silica fume

Table 3.1 Physical properties of silica fume

Properties	Unit	Specification
SiO_2	%	>90%
Loss On Ignition	%	0.03
Bulk Density	kg/m^3	200-350
Specific Gravity	(-)	2.2-2.3
Specific Surface	(m^2/g)	15-30

3.1.2 Sodium Hydroxide

Sodium hydroxide is an inorganic metal base, with very high caustic performance and white color. The molar mass of sodium hydroxide is equal to 39.99 g/mol. The sodium hydroxide used was in pellet form and had 99.0% purity. Sodium hydroxide solutions is prepared by mixing the pellets with distilled water to achieve different concentrations were used in preparing samples.

3.1.3 Perlite

Perlite is a natural pozzolan with high amorphous glassy phase content and is an ideal candidate for alkali activation owing to its high SiO_2 and Al_2O_3 contents and its SiO_2/Al_2O_3 ratio. The perlite used in the tests was obtained from Mollaköy, Erzincan and was ground with a ball mill to a fineness of ~5000 cm^2/g. Its specific gravity was measured as 2.38 g/cm^3. The chemical composition of the perlite used, determined using x-ray fluorescence spectroscopy in METU Central Laboratory, is given in Table 3.2.

Table 3.2 Chemical composition of the perlite used

Component	Percentage
SiO_2	71.8
Al_2O_3	13.8
K_2O	5.49
Na_2O	3.51
Fe_2O_3	1.85
CaO	1.11
Cl	0.126
MnO	0.0886
MgO	0.0380

3.1.4   Expanded Perlite

Normal perlite begins to expand when heated to 850-1100 °C, due to the escape of water inside the structure. Expanded perlite which was used in the experiments was obtained from Etiper Company. The bulk density of this perlite was measured approximately about 140-150 kg/cm^3. The chemical composition of the perlite was tested by x-ray fluorescence spectroscopy in METU Central Laboratory and the result are given in Table 3.3.

Table 3.3 Chemical composition of expanded perlite

Component	Percentage
SiO_2	73.4
Al_2O_3	14.4
K_2O	6.22
Na_2O	3.18
CaO	1.06
Fe_2O_3	1.03
MgO	0.219
BaO	0.146
TiO_2	0.134

3.1.5 Basalt Fiber

Basalt fibers are produced from molten basalt rock made into very thin threads and cut in the desired length depending on the particular usage. High tensile strength and fatigue resistance, high thermal conductivity, high resistance to acids, alkalis and corrosive materials and other properties make basalt fiber suitable for use in materials to be subjected to high temperature and highly alkaline solutions as in this study. Basalt fibers used in the tests were "chopped basalt fiber" from Dost Kimya Company. Technical information about this fiber is given in the Table 3.4.

Table 3.4 Physical characteristics of basalt fiber

Properties	Unit	Specification
SiO_2	%	>90%
Loss On Ignition	%	0.03
Bulk Density	kg/m^3	200-350
Specific Gravity	(-)	2.2-2.3
Specific Surface	(m^2/g)	15-30
Length	cm	2.5

3.2 Mixing and Molding Procedures

This part of the thesis explains the preparing method of samples.

3.2.1 Concentration of Basic Solutions

Samples were prepared using NaOH solutions with 4 different concentrations. For preparing these solutions the sodium hydroxide pellets were dissolved in distilled water. The weight of NaOH used, depended on the desired activator concentration. For example, to prepare an 8M NaOH solution, 320 g of NaOH was dissolved in one liter of water. Mixing was done with a glass stirrer by hand until a homogeneous, colorless solution was obtained. 4, 8, 12 and 16 M concentrated sodium hydroxide solutions were prepared. These solutions were kept in 10-cm-diameter containers with a tight rubber cover, at room temperature (23 °C). The specific weight of each activator solution concentrations is shown in Table 3.5.

Table 3.5 Specific weights of the NaOH solutions used to prepare samples

Concentration (M)	4	8	12	16
Specific Weight	1.11	1.29	1.38	1.48

3.2.2 Solution-to-Powder Ratio

The activating sodium hydroxide solution was mixed with silica fume (powder) at the different ratios given below:

- 50 g solution: 100 g silica fume

- 75 g solution: 100 g silica fume

- 100 g solution: 100 g silica fume

- 125 g solution: 100 g silica fume

3.2.3 Mixing Temperature and Duration

The activating solutions were used in three different conditions:

i. Room temperature (23 ℃): In this group of samples the solution is brought to room temperature prior to mixing with silica fume. For a fixed solution mass, the lower concentration solutions contains higher amounts of water mixing of the 4 M and 8 M mixtures was easier and mixtures were prepared by spatulation. At higher concentration, because of the doughy form of the powder-solution mixture, mixing by hand was easier. Mixing was continued until achieving a homogeneity. There was no time limit for placing the samples in the mold in this method.

ii. Immediate temperature after solving NaOH in water: As previously mentioned, dissolution of NaOH is exothermic and causes an increase in the temperature of the mixture. Higher concentrations resulted in a higher temperature as indicated later in the Table 4.2.

In this group, for samples made with solution temperatures higher than 75 °C, time to cast the specimen is very short and actually, not enough for adequate mixing and most of the time during mixing, the mixture overflows, so working with them was hard.

iii.   At ~70-75 °C: In this method, the solution was heated to ~70-75 °C with an electric heater in a closed container and then mixed with the silica fume. In this process, time to place the mixtures in the molds is very short.

In all these preparation methods, the pastes were mixed until they obtained homogenous structure without any powder form of silica fume powder detectable by eye or any undissolved mass inside the mixtures.

3.2.4 Mixing Equipment

The basic compounds of all samples are silica fume and the sodium hydroxide solutions with different concentrations. Because the mixtures were very sticky and harden rapidly, the mixing operation needed to completed as quickly as possible. The sample mixing was performed inside plastic cylindrical containers of 10-cm diameter and 20-cm height. First, the silica fume was put in the container and then NaOH solution was poured over it and mixed. Other materials, if any, were added subsequently.

3.3 Molding

All samples were prepared in 5×5×5 cm cubic molds. The mixtures tended to stick to the molds, so to prevent breaking the samples during the unmolding, plastic film was used inside the molds. Another important point was to half fill the molds because of the expansive nature of the paste. The weight and volume of each sample was measured at this point.

3.4 Curing

After mixing and molding, the samples were put into the oven for curing. Different curing temperatures and durations were used. Samples were kept in the molds in the oven until they could maintain their shape, which depended on the oven temperature of the oven. After demolding, the weights and volumes of samples were recorded again (without the plastic film). The height, width, and length of each sample was measured to calculate volume. The samples were then put back inside the oven at the

same temperature and kept for different lengths of time. The cohesiveness of the samples increases as they get warmer, so after unmolding again plastic film was used.

3.5   Heat Treatment

The oven cured samples were placed in the oven at higher temperatures for different periods of time and again their weights and volumes were measured. Samples were heated to a maximum temperature of either 200, 300, 400, and 500 °C. The rate of heating was also changed. The heating rate affects the properties of the final product. 4 different heating rate were tested: 1 °C/min, 5 °C/min, 7 °C/min, and 10°C/min. Samples heated at the specified temperatures for 60 minutes and then remained in the oven to cool down to room temperature. Figure 3.2 shows a schematic diagram of the process for preparing foamy specimens.

Preparation of silica fume
and NaOH paste

↓

Mixing other additives

↓

Curing in 100 °C dry oven
for 24 h

↓

Heat treatment in 300-
400 °C dry oven 1 hour

↓

Expanded final product
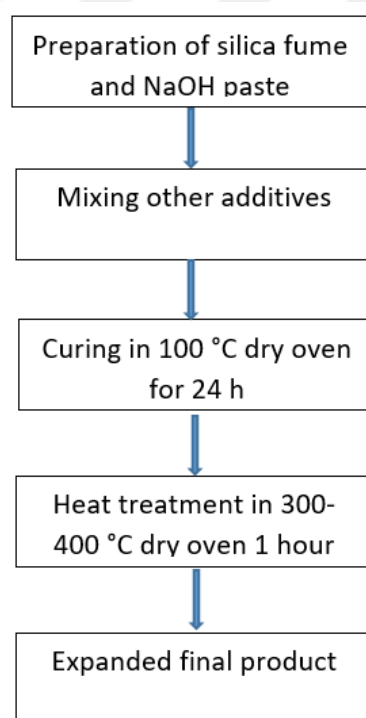
Figure 3.2 Schematic diagram of the process for preparing alkali-activated porous materials.

Two main reasons for the expansion of specimens during the different step of preparation are: (a) The production of H_2 gas by the reduction reaction of water: by increasing the viscosity of samples and consolidation during the alkali activation process produced H_2 gas trapped inside the samples and causes Expansion in the specimens (Equation 3-1).

$$4H_2O + Si \rightarrow 2H_2 + Si(OH)_4 \hspace{3cm} \text{(Equation 3-1)}$$

(b) Production of water: related to the reaction of silanol condensation ($2Si–OH = Si–O–Si$) and the other reason is exothermicity of the reaction involving cold and heat transfer during the reaction.(Prud'homme et al., 2010; Prud'homme et al. 2011)

3.6 Volume Measurement of Final Products

Most of the time, the final product of these steps did not have regular geometrical form and volume measurements was difficult, so Archimedes' water displacement method was used to determine volume. This method uses the differenced in the measured mass of an object in air and under water to determine its volume. To prevent absorption of water, sample was completely covered with 3-4 layers of plastic film. The weight measurement excluded the weight of this plastic film (~5 g). Another factor complicating the measurement was the specific weight of the final products (lower than water), making them float on water, so a heavy object was used to keep the specimen under water.

3.7 Influence of Additives

The final product of these experiments is a material with high porosity and very low density. Certain additives were chosen in a way to reduce the amount of silica fume used in the mixtures without affecting these properties negatively.

3.7.1 Influence of Adding Ground Perlite

Ground perlite was added to the pastes to make the solid structure stronger by introducing some Al content to the system. To investigate the influence of ground

perlite, the powder-to-activator ratio was kept constant and equal to 1, and 10, 20, 40 % by weight of silica fume was replaced with perlite. All the other processes like molding and heat treatments were identical.

3.7.2   Influence of Adding Expanded Perlite

Expanded perlite was added to the mixtures as an aggregate or filler. Because of low specific weight, it seemed to be a good candidate for reducing the cost and increasing durability and strength of samples, without negatively impacting the low density of final products. Some samples were prepared for evaluating the physical effect of this addition to the plain mixture of SF and NaOH. Mixtures with an activator-to-powder ratio of 1 were prepared and expanded perlite was added to this mixture volume ratio of 1/2, 1, and 2.

3.7.3   Influence of Adding Basalt Fibers

Because of the high curing and heat treatment temperature used and also the low density of final products, the use of basalt fibers was deemed is more appropriate than other fibers. For example, steel fibers have higher specific density than basalt fiber which would increase the density of final products. Synthetic fibers have very low density but their low melting points (max. 200-300 °C) make them an unsuitable. Basalt fiber was added as 1 % and 2 % of the total sample weight.

3.8   Experiments

In this section, all tests performed on the samples are briefly explained:

3.8.1   Mechanical Tests

Compressive strength test was measured on cubic expanded specimens which cut from uniform (in terms of porosity, determined visually) parts of final products, so samples used in this test did not all have identical dimensions. Specimens used have the cubic shape with the dimensional ratio ~1. The universal testing machine (MTS) in the Material of Construction Laboratory at METU was used to determine compressive strength. Deformation-controlled loading was performed, at a rate of 10 mm/min.

3.8.2 Scanning Electron Microscopy

Scanning electron microscopy (SEM) is a method used to investigate the surface and texture of solids and gives high-quality images that have a higher magnification and a higher depth of field compared with most other imaging methods like optical microscopy. The main technique in SEM is to irradiate an electron beam to the surface of samples and detect the secondary electrons emitted and use them to build up an image of the surface. Another useful way to use a SEM is for nondestructive chemical analysis (EDX). The basis of this analysis is the interaction of primary electrons with the surface of sample and emission of x-rays. The energy and intensity of these x-rays are measured by an x-ray detector to determine the chemical composition of the magnified part of the sample. SEM imaging of the samples was performed in the Central Laboratory of Middle East Technical University using a QUANTA 400F Field Emission SEM. Samples were oven dried at 80 °C for 24 hours and the surface covered with an ultrathin layer of gold to improve the imaging result and strengthen the secondary electron signal. Figure 3.3 shows the different responses of a sample surface to incident electros.
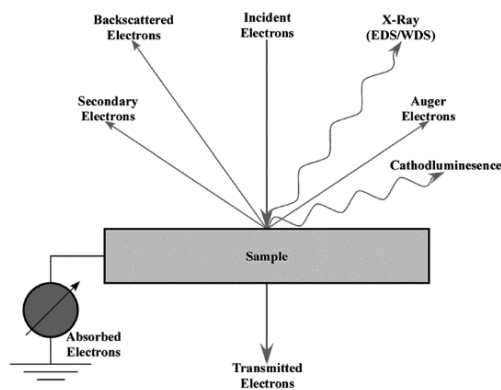

Figure 3.3 Different response of a sample surface to incident electrons

SEM analysis was performed on 4 samples with different mixture properties, listed in Table 3.6.

Table 3.6 List of samples analyzed by SEM

Sample	Powder	Solution	Solution / Powder
1	Silica fume	4 M NaOH	1
2	Silica fume	12 M NaOH	1
3	Silica fume	16M NaOH	1

3.8.3 Computed Micro Tomography (µCT) Scanning

Computed micro tomography scanning is a method, similar to medical CT scans, that can be used on materials like ceramics, rocks, metals and many others at very small scales. By application of X-rays and without destructing the samples, information about the 3-D structure of samples, interior cracks and pores can be obtained. The basis of this method is to generate 2-D images (slices) in different sections of the object and transform these 2-D projections to a 3-D picture of it. The µCT scans were performed at the National Institute for Standards and Technology, Boulder, CO, USA.

3.8.4 Nitrogen Adsorption Test

One of the most popular ways to study the surfaces of porous materials, their specific surface areas, and their pore size distribution is gas adsorption. Most of the time nitrogen (N_2) is used as an adsorbate because it is cheap and it has low reactivity with most solids and can be easily found in pure gas or liquid form. The first step of the test is to vacuum contaminants and vapors adsorbed from the air onto the samples. Then, the surface of the sample is covered with a layer of adsorbent molecules named a monolayer, then as the test goes on the thickness of gas increases to several molecules and multilayer adsorption happens. By continuing adsorption, smaller pores fill earlier than others (Aligizaki, 2005; Jaroniec et al., 1999). For this test 3 samples were tested with a Quantachrome Autosorb-6 at METU Central Laboratory. The volume of adsorbed gas has an inverse relationship with the temperature of the vapor, so this test is done at the boiling temperature of liquid nitrogen (77.3K or -195.7℃) (Aligizaki, 2005).

3.8.5 Particle Size Distribution

The grain size of studied materials can impact characteristic of final materials (Xu et al., 2007). One of the commonly used and useful methods for particle size measurement is low-angle light scattering (laser diffraction) especially because of its advantages such as short testing time (~ 30 min), high accuracy, a wide range of particle size measurement and high quality. The basic technique of this method is to study the light reflected and absorbed by the particles. Mie theory is used to determine grain size from light reflection. This test was performed on the silica fume used at the METU Central Laboratory using a Malvern Mastersizer (Hydro) 2000 machine. The analysis was done in "wet mode" using water as a dispersant to suspend the particles.

3.8.6 Nuclear Magnetic Resonance Spectroscopy (NMR)

Unlike in any of the other methods, in the NMR tests, the nuclei of the atoms are studied. Most of the time the nuclei of atoms with an odd atomic number or nuclei which have spins are appropriate for NMR because of their magnetic properties. In these kinds of nuclei, energy transfer happens when exposed to the electromagnetic field. Simply frequency of electromagnetic field is needed to change the basic energy level to the higher one, and these changes are measured by different methods (Aligizaki, 2005). This test was performed with a Bruker Superconducting FT.NMR Spectrometer Avance TM 300 MHz WB in the METU Central Laboratory. Samples were whirled at a spin rate of 8500 Hz on a 4 mm MAS rotor to make the magnetic field feel homogeneous. Figure 3.4 shows the different steps of preparation of samples, on which NMR and IR spectra tests were performed.

3.8.7 Fourier Transform Infrared Spectroscopy (FTIR)

Fourier transform infrared spectroscopy is a fast, easy and inexpensive method of studying the nature and concentration of molecules and bonds inside solid samples. Each chemical bond has characteristic vibration frequencies. Different beams of infrared light are sent to the samples and only the light with the same frequency as

that of the bond is absorbed. Each absorbed wavelength and amount of absorption stands for a specific bond and by analyzing these result chemical bonds inside the materials is specified. A Bruker FRA 106/S in the METU Central Laboratory was used for these tests. Figure 3.4 shows the preparation procedure used for the FTIR samples.
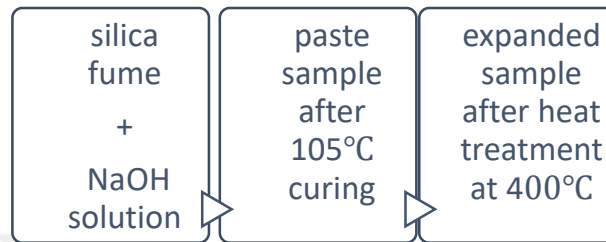

Figure 3.4 sample preparation for NMR and FTIR spectroscopy

3.8.8   Water Absorption

Water absorption test was performed on the heat-treated (expanded) final products to evaluate their durability against water. The results of this test could reveal the volume of pores and as a result the porosity of the specimens. Oven dried samples were immersed in water (using heavy objects to keep the sample submerged) and weight of the surface dry samples measured at specific intervals (ASTM C 642, 2013). In the first 24 hours, the measurement intervals are kept short due to the rapid change in absorption and after that, measurements were performed once every 24 hours.

If the weight of oven dried sample named as A and the weight of the final surface dry sample is B the percentage of water absorbed is calculated as:

% of water absorption $=(\frac{B-A}{A})*100$ Equation (3-2)

30

CHAPTER 4

RESULTS AND DISCUSSION

In this chapter, the results of all experiments mentioned in Chapter 3 are presented and discussed.

4.1   Influence of Sodium Hydroxide Concentration and Mixture Proportions on Bulk Density

Several different combinations of silica fume and sodium hydroxide solution were prepared and their density and homogeneity evaluated to choose an optimum combination to use for the other tests. Homogeneity of final products was evaluated visually inspection. The bulk density reported for samples is the average of two mixtures were prepared. First, the NaOH solution was added to the silica fume at room temperature (23 °C) and mixed by hand. The paste obtained was cured at 100 °C in a dry oven for 24 hours, and then heat treated at 300 °C for 120 minutes. In the first 60 minutes, oven (and samples) is heated to 300 °C at a rate of 5 °C/min. Then, in the second 60 minutes, the oven was kept at constant temperature. The volume and mass of the samples were measured only after the oven cooled to room temperature. Table 4.1 lists the bulk densities measured on the various heat-treated (expanded) samples.

Table 4.1 Bulk density (g/cm³) of samples made using different activator-to-powder ratios (A/P)

NaOH Solution Concentration (M)	A/P=0.5	A/P=0.75	A/P=1	A/P=1.25
4	Sample broke	Sample broke	0.402	Sample broke
8	0.575	0.297	0.261	0.139
12	Could not be mixed	0.214	0.092	0.053
16	Could not be mixed	0.201	0.095	0.074

In this method because of the very low amount of water in pastes with A/P = 0.5 using the 16 M solution, it was not possible to reach a homogeneous paste, and some powder remained unreacted, so it was not possible to mold and continue the tests. On the other hand, the 4 M samples with A/P = 0.5 and 0.75, because of their very low amount of activator and inadequate activation after 24 hours of curing, broke down to the pieces. As seen in Table 4.1 the lowest density belongs to the 16 M, A/P = 1.25 but the porosity in this sample was not sufficiently homogenous. This sample transformed (upon expanding) a hollow shell and is an inappropriate selection for rest of studies. 4 M samples have better homogeneity but higher density. 8 M samples could be used as a binder because they do not have a porous structure. Just a few pores in 1-1.5 cm in diameter obtained at lower proportions and in A/P = 1 and 1.25 these holes were connected and make a bigger hole. Because of the unsatisfying result obtained all the solution concentrations, and from economical point of view due to the higher usage of activator and, A/P=1.25 was omitted in the rest of the experiments. As A/P increases, at all the solution concentrations, the final products have a foamier state. Figure 4.1(a) shows the differences in expansion of samples made with different solution concentrations at A/P = 1. Figure 4.1(b), (c), (d), (e), and (f) show the cross sections of these specimens allowing the homogeneity of the pores in the specimens to be compared.

Figure 4.1 (a) Size comparison of different solution concentrations, (b) cross section of different solution concentration, and cross section of (c) 4 M, (d) 8 M, (e) 12 M, and (f) 16 M.

(d)

(e)

Figure 4.1 continued

(f)

Figure 4.1 continued

4.2 Influence of Curing Temperature and Duration on Bulk Density

In this part of tests, a comparison between several curing temperatures and duration was done. A mixture with A/P = 1 was prepared using a 12 M activating solution and cured at 60 °C, 80 °C and 100 °C for 6, 12, 18 and 24 hours and heat treated at 400 °C with rate of 5 °C/min. The change in the volume and density of samples during various production steps was investigated and the results are given in Figure 4.2 and Figure 4.3.
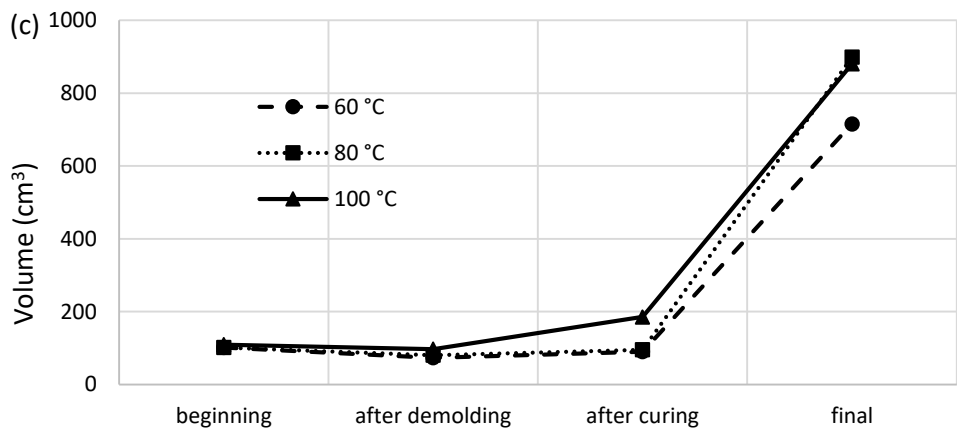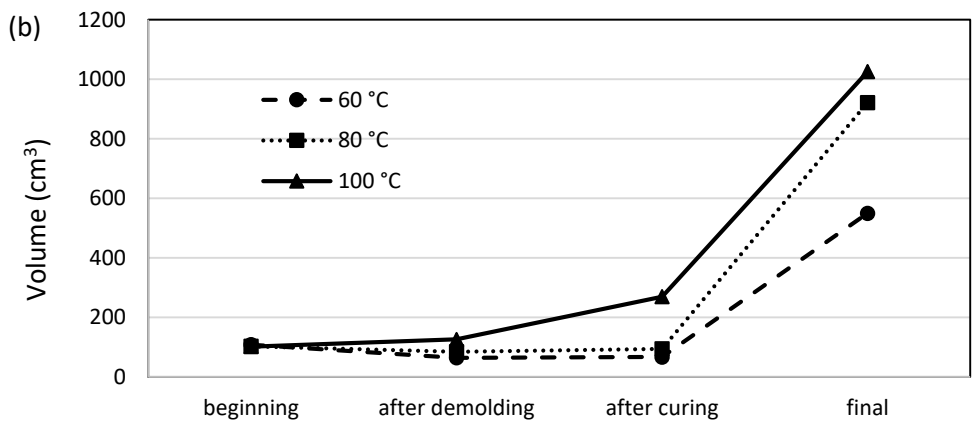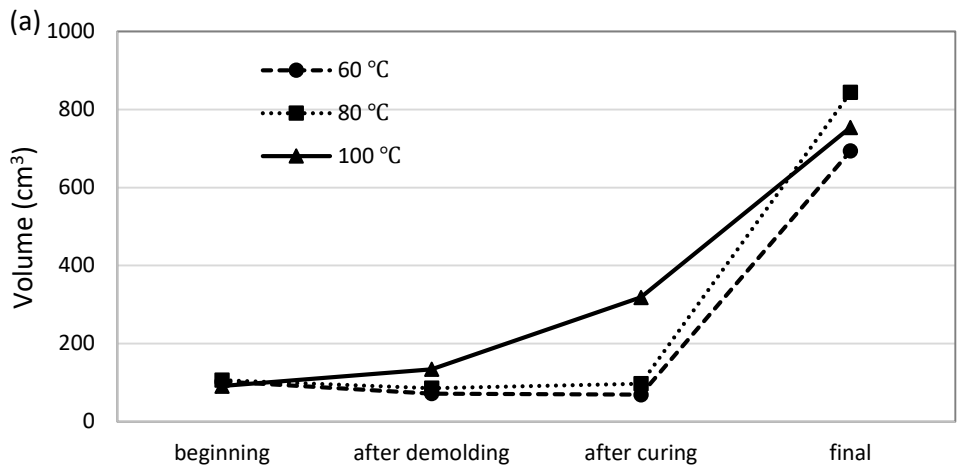
Figure 4.2 Volume expansion of 12 M mixture after (a) 6 hours, (b) 12 hours, (c) 18 hours and (d) 24 hours of curing
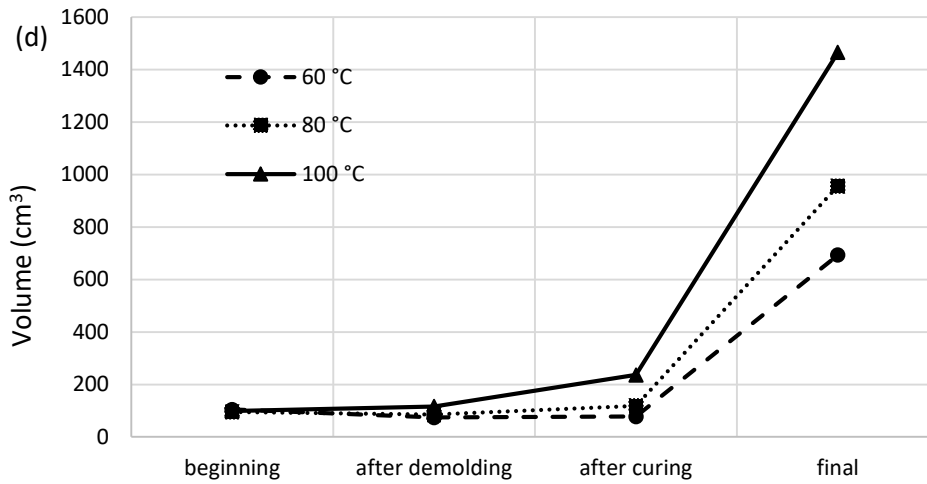
Figure 4.2 continued

The final volume of the samples is seeming to be related to the curing time and duration. Volume increases continuously in 100 °C-cured samples during the curing period, but at 60 °C and 80 °C not only is volume constant during the curing period but also in some cases, a slight contraction is observed. In 60 °C cured samples contraction continues during the entire curing period, but samples remain intact. On the other hand, 80 °C-cured samples contracted until the demolding stage and expansion was observed afterwards. In all stages, these samples remained solid but flexible.

 The final densities of samples are also compared in Figure 4.3. It was observed that, the final density of 60 °C-cured samples is approximately constant, independent of the curing duration, and also is the highest among all other curing temperatures. The 80 °C-cured samples expanded somewhat two-dimensionally owing to their plastic nature (Figure 4.4 (b)). Final density appears to have an inverse relation with curing duration. The greatest expansion was observed in the 100 °C-cured samples curing at higher temperatures than 100 °C (e.g. 120 °C) gave products similar to the 100 °C-cured samples. Figure 4.4 (a) also shows the final product of different curing duration and period and the b part of this figure also indicates the cross section and pore status in the samples.
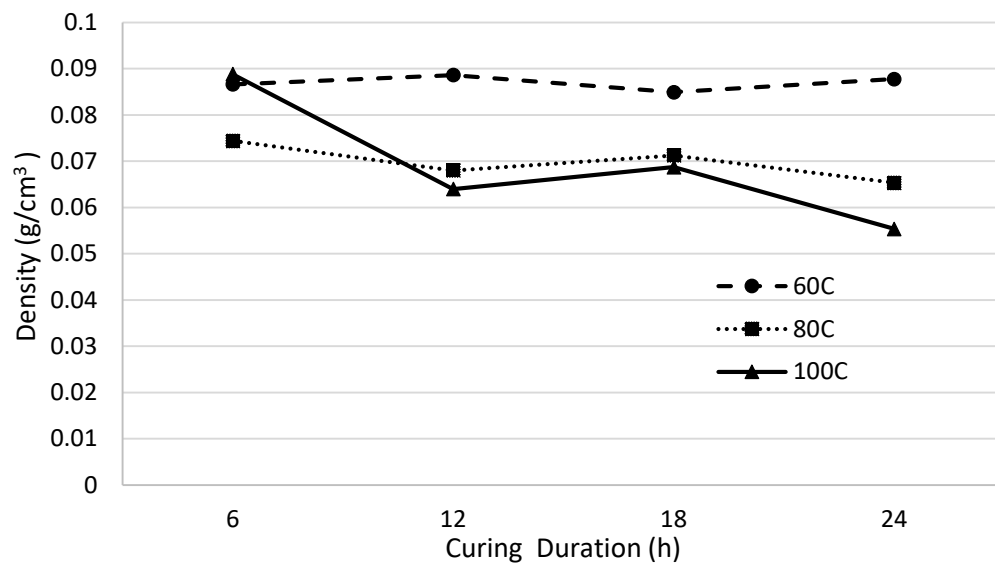
Figure 4.3 Final density of samples cured at various temperatures for different durations
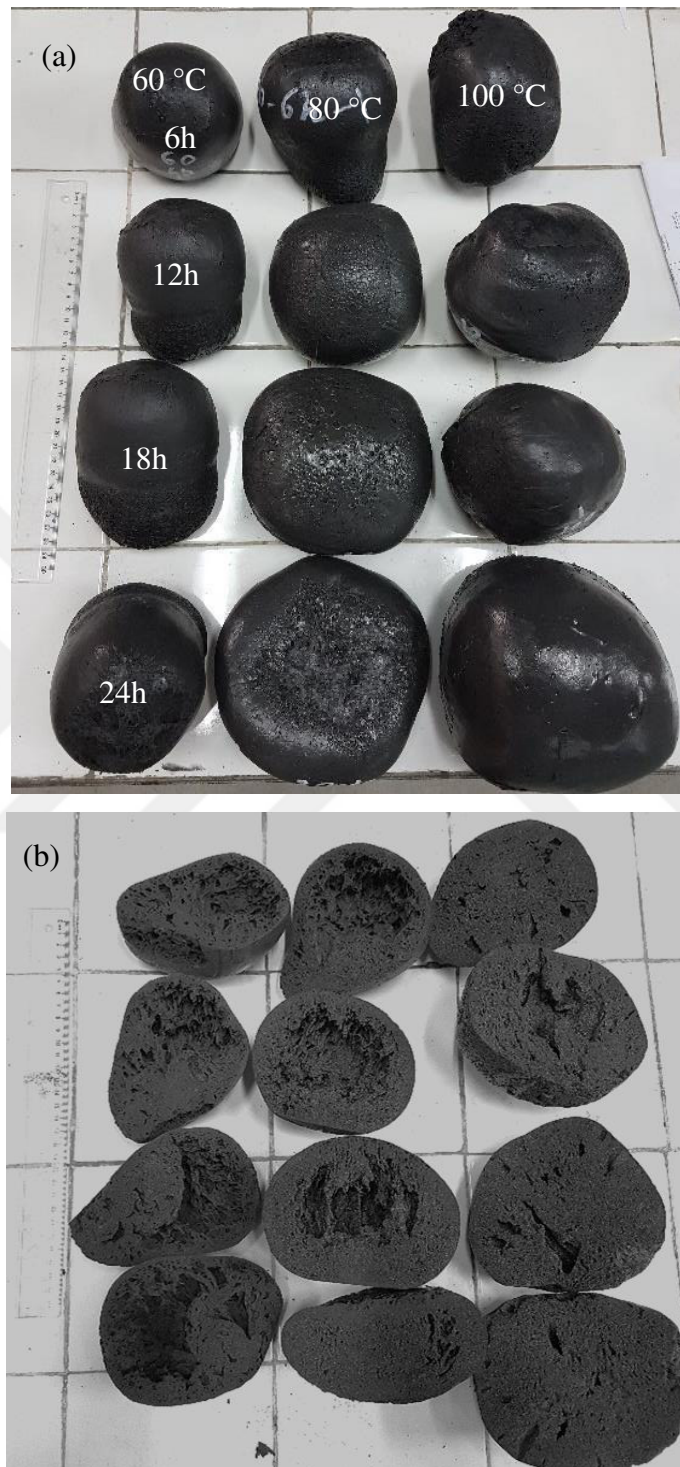
Figure 4.4 (a) Size of samples made using 12 M activating solutions, cured at different temperatures, (b) cross sections of the samples in (a)

4.3   Influence of Mixing Solution Temperature on Bulk Density

Mixtures which were prepared at room temperature had stiff doughy form and reaching a uniform state was hard and required great effort. Another problem was the extension in the demolding period (up to 4 hours). For overcoming these problems in the next stage of experiments different mixing temperatures were tested. As it was mentioned in Chapter 3 dissolving sodium hydroxide in distilled water is an exothermic reaction and higher concentration of solution gives a higher final temperature. The temperature of each concentration was recorded in the Table 4.2.

Table 4.2 Temperature of NaOH solution as mixed in distilled water

Concentration (M)	4	8	12	16
Temperature (°C)	55	75	100	105

Combining the NaOH solution with silica fume at these temperatures leads to different behavior during the mixing period.

The mixing process and molding are easier since the paste converted into a viscous liquid. The 8 M mixture solution at 75 °C is particularly fluid and uniform and the time of curing until demolding decreases to 90 min indicating faster stiffing. It was observed that with higher concentrations at higher temperatures adding silica fume causes boiling and over flowing in the initial stirring stage and the hardening period decreases to 3-4 minutes taking place prior to oven curing. From experience gained about the mixing and stiffening of the mixtures made with different proportions and at different temperatures, 75 °C was chosen as the mixing temperature and solutions of all concentrations were brought to 75 °C prior to mixing with silica fume. Density measurements of samples made using activating solutions with three different concentrations, at different temperatures are shown in Figure 4.5. Samples cured at 100 °C for 24 h and heat treated in 300 °C.
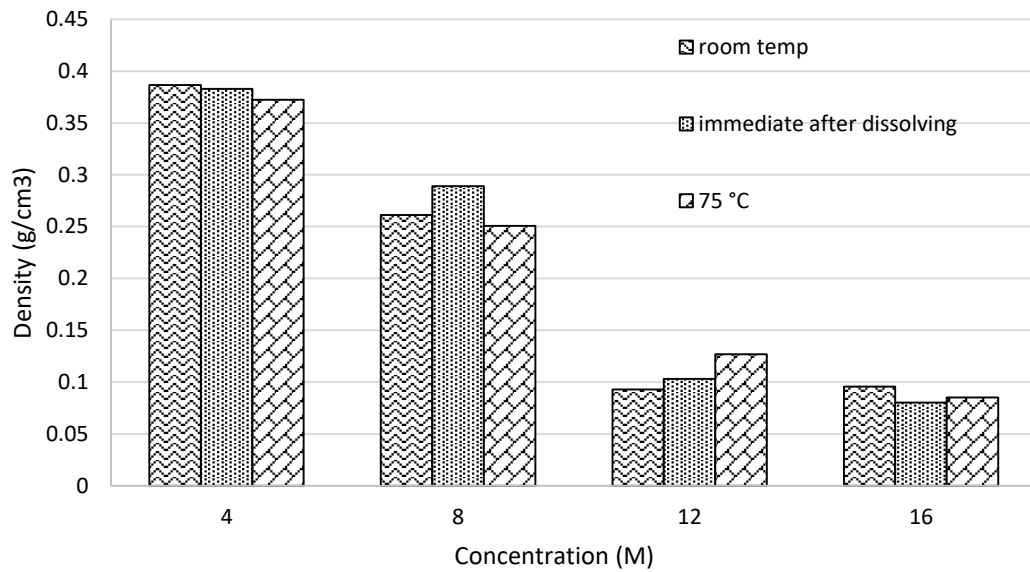
Figure 4.5 Density of the different solution concentrations in different mixing temperatures (A/P = 1 for all the mixtures).

In all mixtures A/P = 1. A comparison of these results indicates that mixing temperature does not impact the density of the final product greatly especially when higher concentration solution is used and it is because of greater expansion of final products, so higher temperatures just make the mixing process easier and faster.

4.4   Influence of Heat-Treatment Temperature

The most important and effective part of the production process is the heat treatment because the greater part of the expansion happens at this stage. Also, because of the high temperature used, it can affect the economics of the production process. The main goal of the heat treatment step is to achieve a greater volume sample with a foamier structure (very small and homogeneous pores). Fewer centimeter-sized pores and a greater amount of mm-sized or smaller pores are desired to give lightweight samples with better mechanical and thermal properties. The influence of different heat-treatment temperatures on the density of final products was investigated. The rate of heating for all the samples was constant and equal to 5°C/min. Samples made using

41

activating solutions with different concentrations, and A/P = 1 were compared and the results are shown in Figure 4.6.
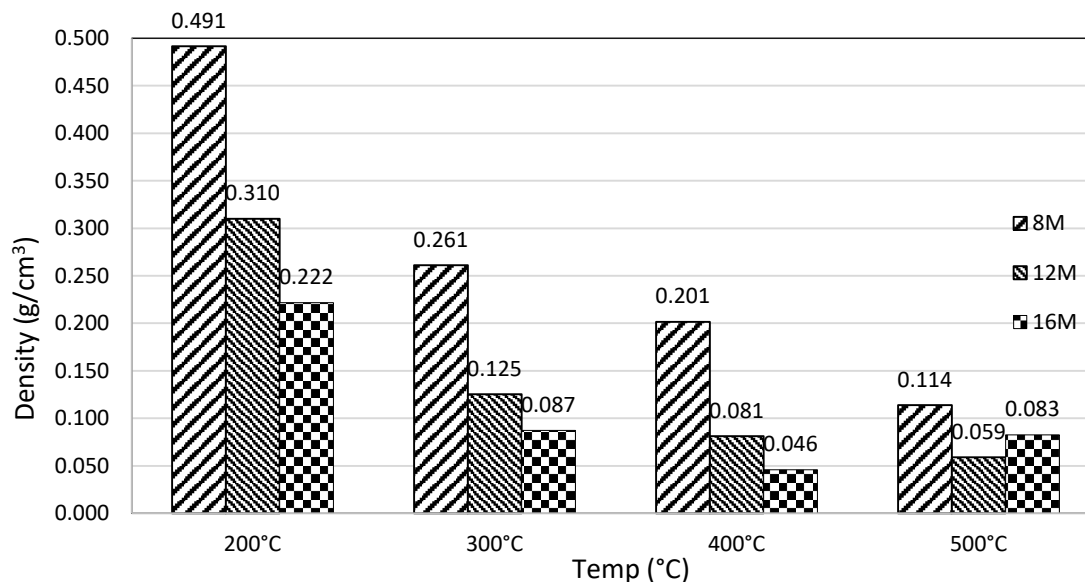

Figure 4.6 Influence of heating temperature on density

Increasing the heat treatment temperature results in lower density final product due mainly to a volume increase. The change in mass is negligible. However, this volume increase causes large holes inside the samples for some of the heat treatment temperatures and solution concentration combinations. The foamy uniform structure with low density is decided as 400 °C for the 12 M samples, and as 300 °C for the 16 M samples.

4.5   Influence of Heating Rate

All prior tests were done at a heating rate of 5°C/min. The effect of the heating rate on the expansion of 12 M solution, A/P =1 samples is shown in Figure 4.7. All the samples cured at 105 °C for 24 hours.
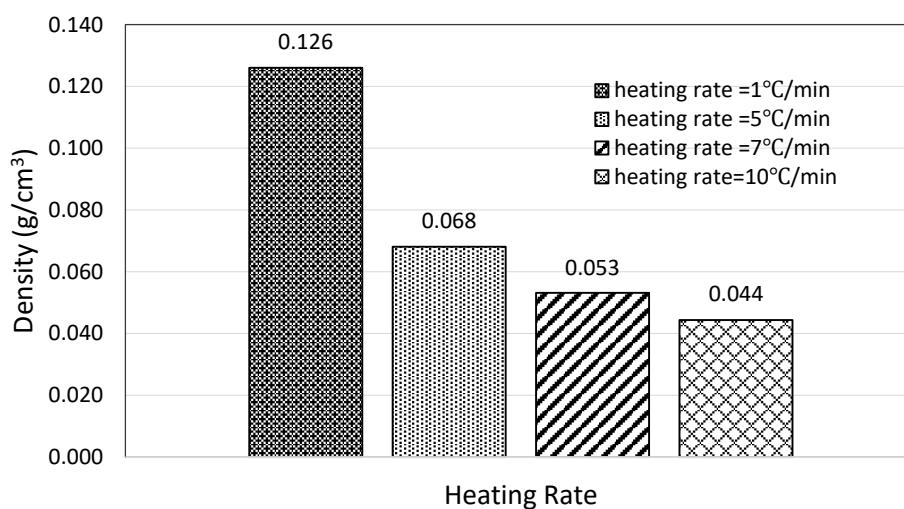
Figure 4.7 Influence of heating rate on the final density of 12 M concentration solution, A/P = 1 samples

The maximum temperature used for these comparative tests was 300 °C. It is observed that the density of the final product has an inverse relation with the heating rate. On the other hand, increasing the rate of heating beyond a certain value was observed to result in a non-homogenous pore structure. The optimum heating rate was considered to be 5-7 °C/min.

After all the investigations on the influence of mixtures and processing parameters on volume expansion and the density and uniformity of the final products (Sections 4.1-4.5), the most favorable parameters were determined and all subsequent samples were prepared accordingly. Figure 4.8 briefly summarized all the preparation tests and the most acceptable results shown in the shaded form.
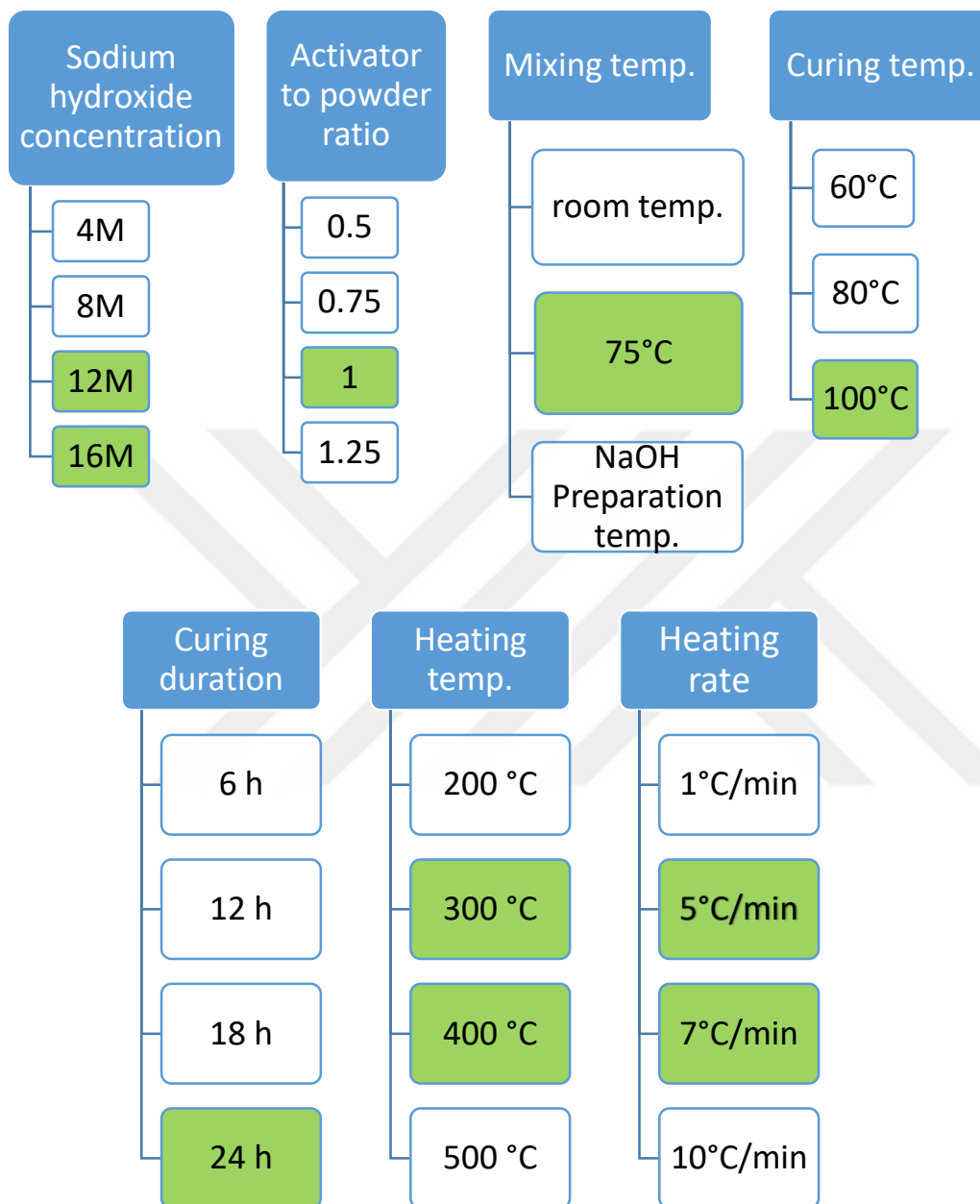
Figure 4.8 selection of optimum sample preparation parameters and procedure (the shaded squares indicate the favorable selections

4.6 Influence of Adding Ground Perlite

Properties of perlite pastes activated with sodium hydroxide solutions and expanded with heat treatment have been investigated by Erdoğan (2015). Based on this part of

the study, ground perlite was added to the mixtures at various percentages. Samples containing 10%, 20% or 40% of ground perlite (by weight of powder) activated at 12 M or 16 M NaOH solutions and A/P = 1 were prepared. The final densities of samples cured at 100 °C for 24 h, and heat treated at 300 and 400 °C, is given in Figure 4.9.
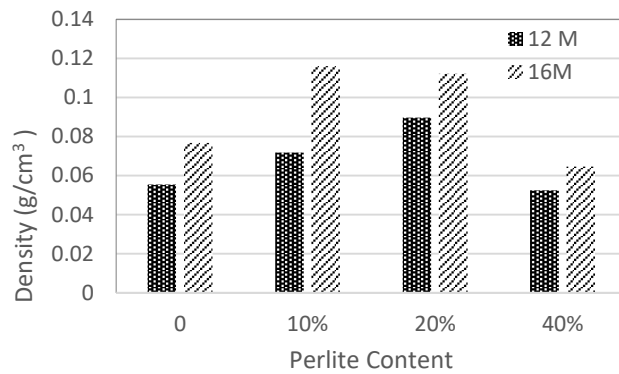

Figure 4.9 Effect of adding ground perlite on density of the final product

Adding perlite in most of the cases caused an increase in density, but this increment decreased beyond a certain addition level (Figure 4.9). Also Figure 4.10 (a) and (b) shows the changes in the size and distribution of pores inside the samples with the addition of ground perlite. The larger pores in the center of the samples grow as the perlite amount increases in the mixtures with both solution concentrations.
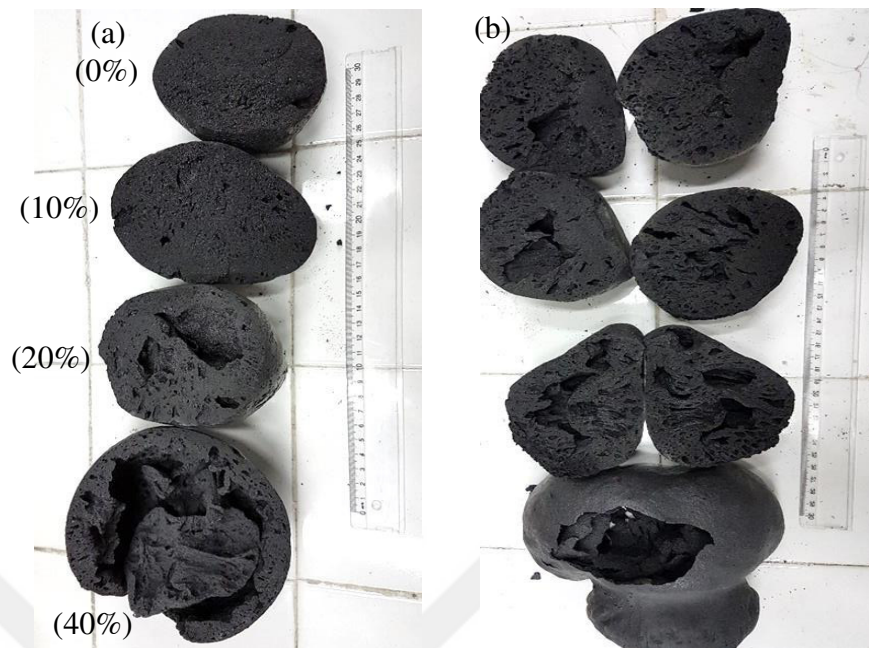
Figure 4.10 Perlite added samples: (a) 12 M, (b) 16 M

All in all, combining silica fume and ground perlite in the mixtures does not improve the properties of the obtained product but also causes problems during the preparation of samples. One of these problems was an extension in the stiffening period for demolding the samples, contains 40% perlite. As mentioned in Section 3.4 samples were demolded after 60-90 min of curing, but adding perlite extended this period, to greater than 6 h in the 40% perlite sample.

4.7   Influence of Adding Expanded Perlite (EP)

The goal of expanded perlite addition to the mixture was to control the pore size and increase the homogeneity of the samples and also improve the mechanical properties of the mixture, because expanded perlite acts as a very light aggregate and filler in the mixture. Expanded perlite was added to the mixture EP: SF plus activator at a volume ratio of 1/2, 1, and 2. Contrary to the expectation, adding expanded perlite reduced homogeneity of the samples, since the lower-density expanded perlite segregated toward the top part of the sample, during mixing. Figure 4.11 shows the cross sections

of EP added samples activated with 12 M and 16 M NaOH solutions cured at 100 °C for 24 h.
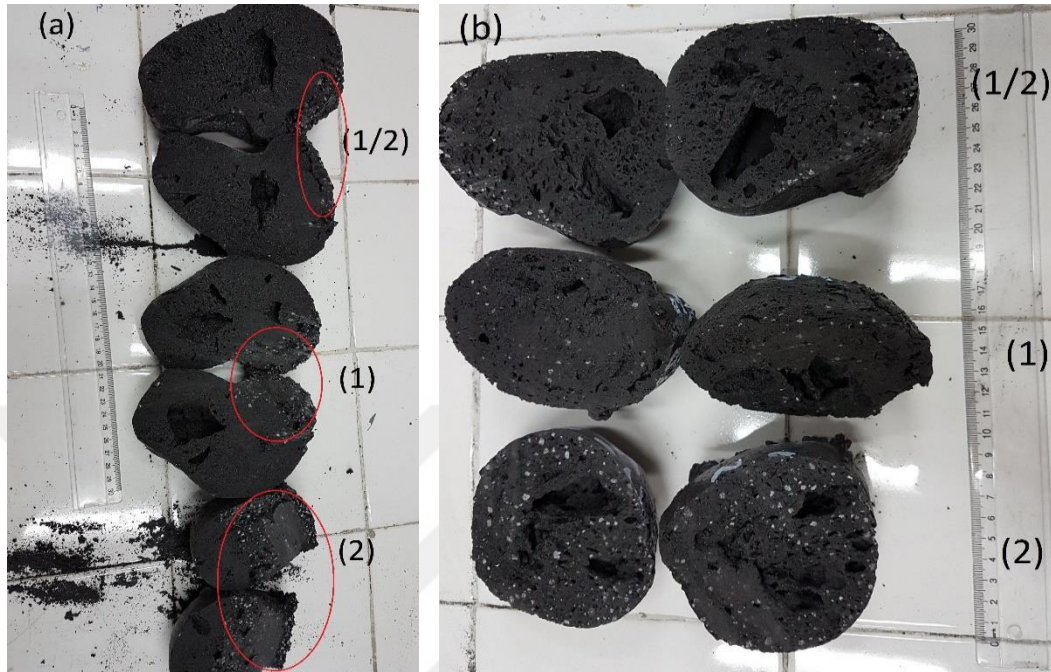

Figure 4.11 Expanded perlite added to samples made using (a) 12 M, (b) 16 M activating solution

Clearly, it is seen in Figure 4.11 that for the 12 M solution samples the segregation and reduction in uniformity is more than for the 16 M samples. Also, addition of EP affected the volume expansion negatively, especially in the 12 M samples. It is possibly because gas water vapor that cause the expansion of sample cannot push the expanded perlite. In Figure 4.12, the bulk densities of these mixtures are compared.
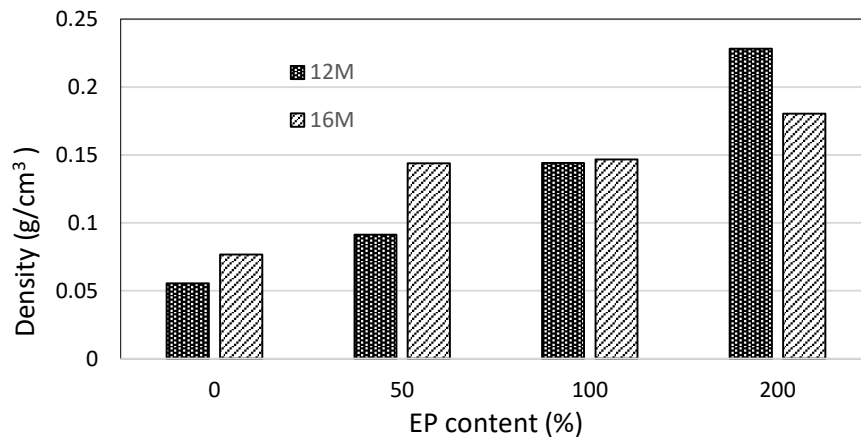
Figure 4.12 Effect of expanded perlite addition on density of the final product

A direct relation between EP content and density was found and this is mainly because of reduced volume expansion in the EP containing samples. Another possible factor is that the bulk density of EP is greater than the bulk density of the final products made without any EP. Hence, EP could only be expected to increase the final densities. But, that the final density exceeds that of the EP indicates that reduced expansion must be the dominate factor.

4.8 Influence of Adding Basalt Fiber on Bulk Density

The aim of adding basalt fiber to the mixtures is increasing the durability and compressive strength of materials by controlling the pore structure of products, so fibers were added to the mixtures in 1% by weight and 2% by weight in A/P=1 solutions and in 12 M and 16 M concentrations. Samples cured at 100 °C and heat treated at 300 °C and 400 °C respectively. Figure 4.13 indicates the expansion changes by increasing fiber content in the 12 M solution samples.
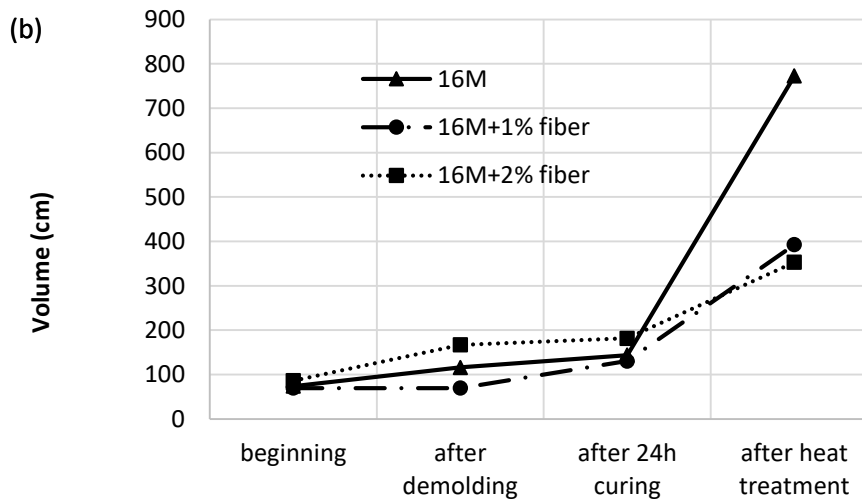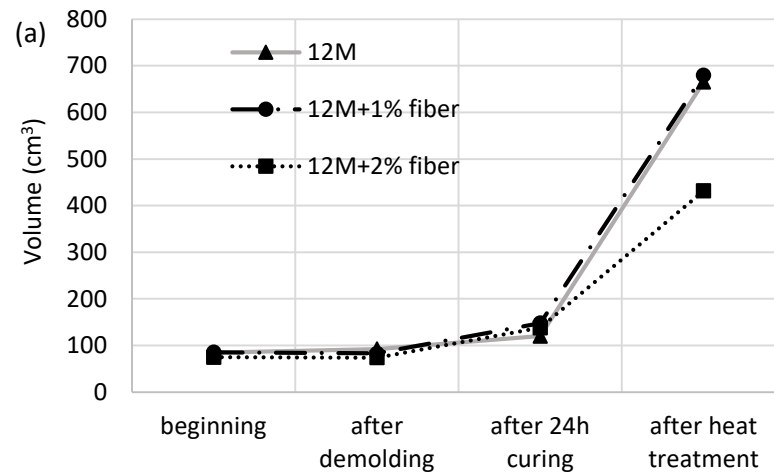
*Figure 4.13 Volume expansion of samples incorporating basalt fiber made with (a)
12 M, (b) 16 M NaOH solutions*

Adding basalt fiber to the mixtures reduces the final volume of the samples especially
that of the 16 M sample. This is expected because fibers increase the tensile strength
and counter the expansion. The other reason for lower expansion in the basalt fiber
added specimens could be the reaction at the surface of fibers in high alkaline media
of samples. Increasing the fiber content increasing the resistance hence 2 % fibers give
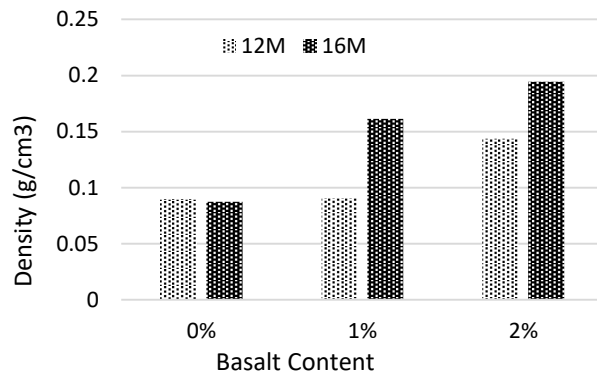a lower expanded volume than 1 % fibers, in both samples.

Figure 4.14 Density of samples with basalt fiber

As a result of the limited expansion, the density of the samples materials also changes by adding fibers does not have as great an effect on 12 M samples as on 16 M. Adding 2 % of fibers increases density two twice that of fibreless samples (Figure 4.14).

Table 4.3 is briefly showing the effect of each additive on the density, uniformity and strength of samples.

Table 4.3 Influence of additives on characteristic of specimens

Additive	Density	Homogeneity	Strength
Ground Perlite	⬆	⬇	⬇
Expanded Perlite	⬆	⬇	⬆
Basalt fiber	⬆	⬆	⬆

4.9 SEM Analysis

Four samples were chosen to be analyzed with SEM imaging: the sample with the lowest density, a denser sample, the sample visually assumed to have the most uniform interior, and sample with perlite. The following sections discuss some of the images. EDX analysis was also performed on certain areas of the sample images, circle on the images indicated the areas over which EDX analysis was performed. The curing temperature and duration and heat treatment temperature of the samples in the following sections, were chosen as those determined to be the optimum values (Figure 4.8)

4.9.1 Sample Made with 4 M Solution and A/P = 1

The mixtures made with A/P=1 and the 4M concentration solution, gave the densest product. Figure 4.15 shows two different points with this sample imaged at different magnifications. An irregular porous structure is revealed, containing many pores smaller than ~50 µm and several much larger (100 of µm) pores. The pores are generally non-spherical with many appearing to be connected to each other (Figures 4.15 (a) and (b)). Areas in Figure 4.15 (c) appear free of smaller pores and indicate of possible melting or softening of the structure during heat treatment. Many small (< 10 µm width) cracks are noticeable in these areas (Figure 4.15 (d)). These cracks and the abundance of shards in the imaged areas are probably due to shrinkage that took place during the cooling period after heat treatment. The porous structure is unable to resist cracking much like the damage observed in aerogels during ambient-temperature drying. Elemental composition measured inside one of these cracks (Figure 4.15 (e)) is shown in Table 4.4.
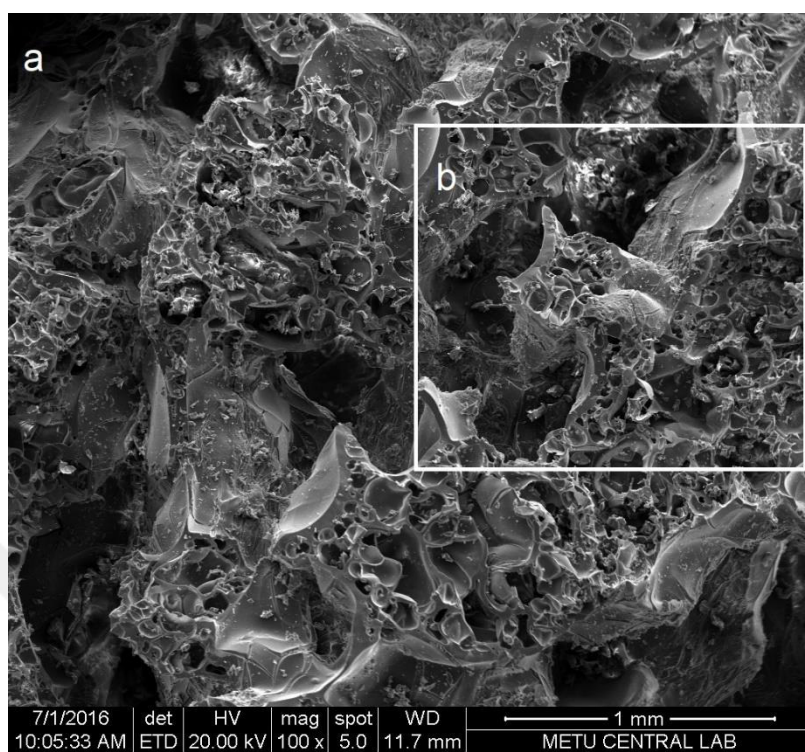
Figure 4.15 SEM images of a sample made with the 4 M activating solution: (a) 100 × magnification, (b) 200 × magnification, (c) another point of sample with 100 × magnification, (d) 500 × magnification of (c), (e) 2000 × magnified of (d)
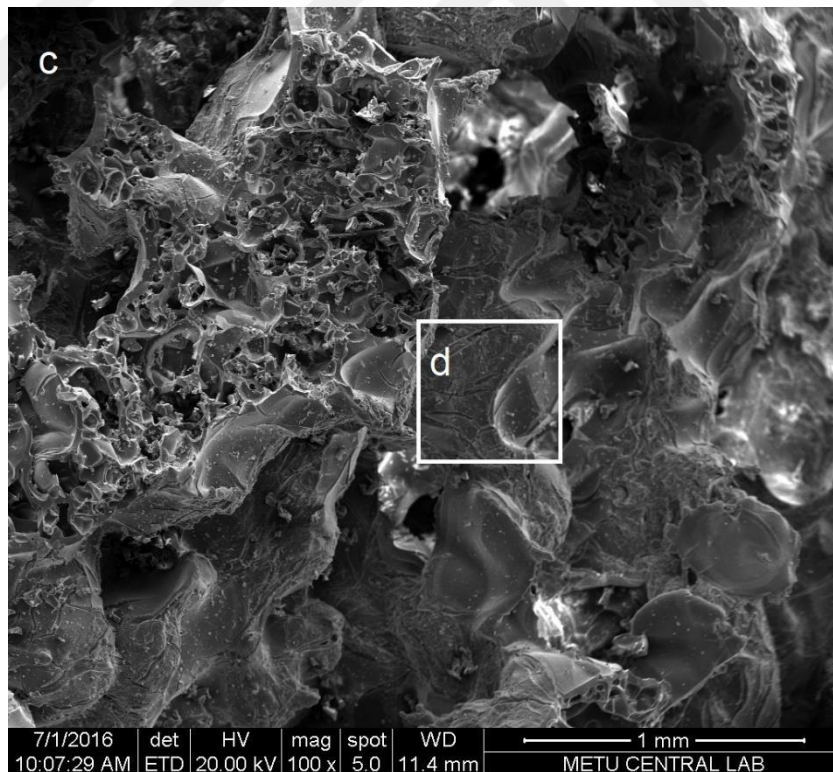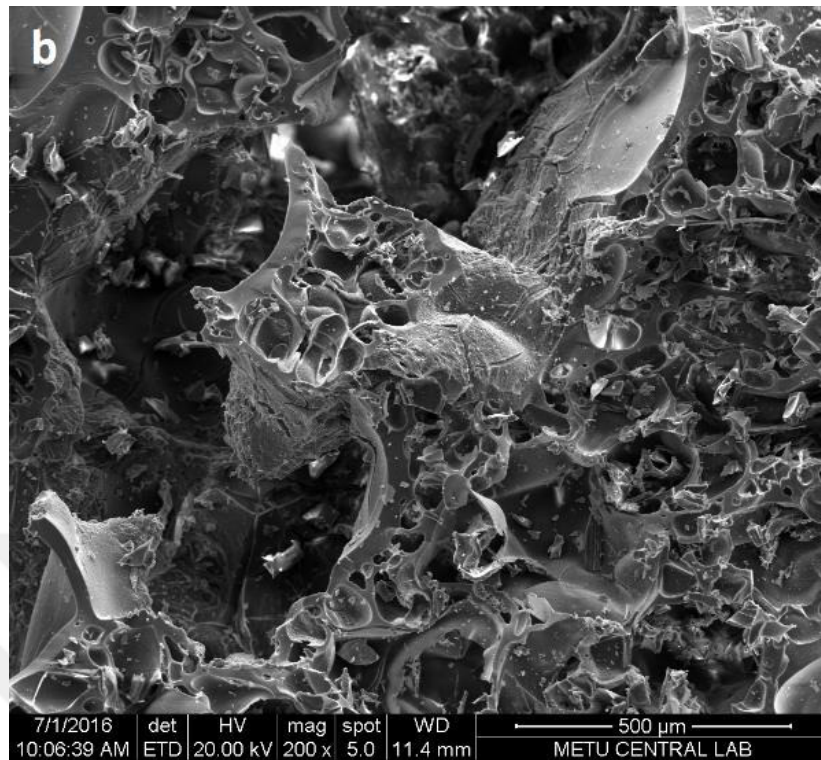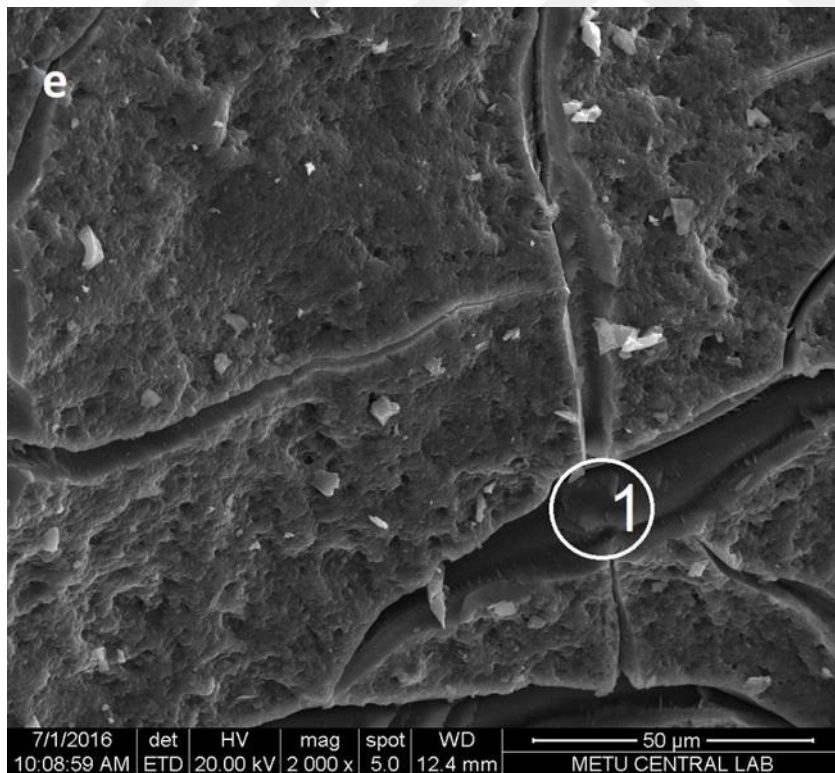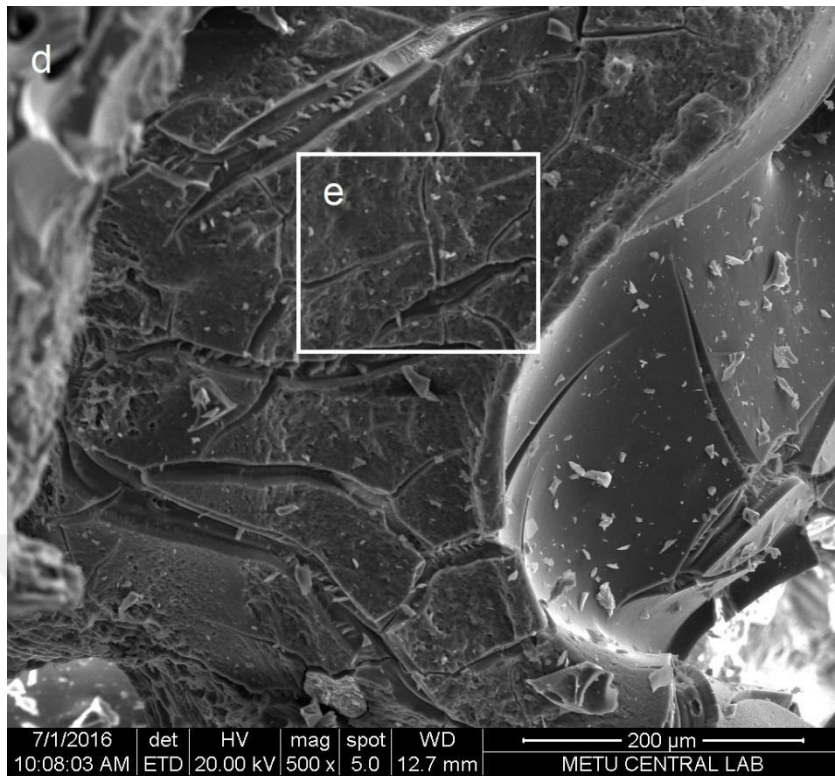
Figure 4.15 continued

Figure 4.15 continued

Table 4.4 Elemental composition for point 1 in Figure 4.15 (e)

element	Si	O	Na	K
1 (wt.%)	47.64	41.34	2.81	0.88

As expected, part 1 is made up of mostly Si and O atoms, with the amount of Na atoms being low due to the dilute 4M activating solution used.

4.9.2 Sample Made with 16M Solution and A/P = 1

This sample was the lowest density sample. Figure 4.16 (a) shows that the interior of this sample is similar to that of the sample activated with the 4 M solutions but perhaps more uniform, containing many small and large pores. Both the smaller and larger pores, however appear to be larger than those in Figure 4.15 (a). Again many shards are visible, indicating damage to the glassy structure during cooling. Several hollow spherical formations (Figure 4.16 (c) and (d)) are visible, some with cracked surfaces. These are likely the pores formed upon expansion of the samples due to loss of water vapor from the polycondensation of – OH groups. EDX analysis was performed at two points in the sample. (Figure 4.16 (a) and (c)). Comparing their elemental compositions with that of point 1 in Figure 4.15 (e) an increase in the Na contents noticed, and it is an expected change because of the increase in the concentration of the activating solution (Table 4.5). a reduced Si/O is also noticeable. The thickness of the typical pore walls inside the samples was measured as 2-3 µm, even smaller pores (<100 nm) are also visible inside the pore walls (Figure 4.16 (e)). Figure 4.16 (c) and (d) show that the pore walls are so thin that they are somewhat translucent.

Table 4.5 Elemental composition for 16 M, A/P =1

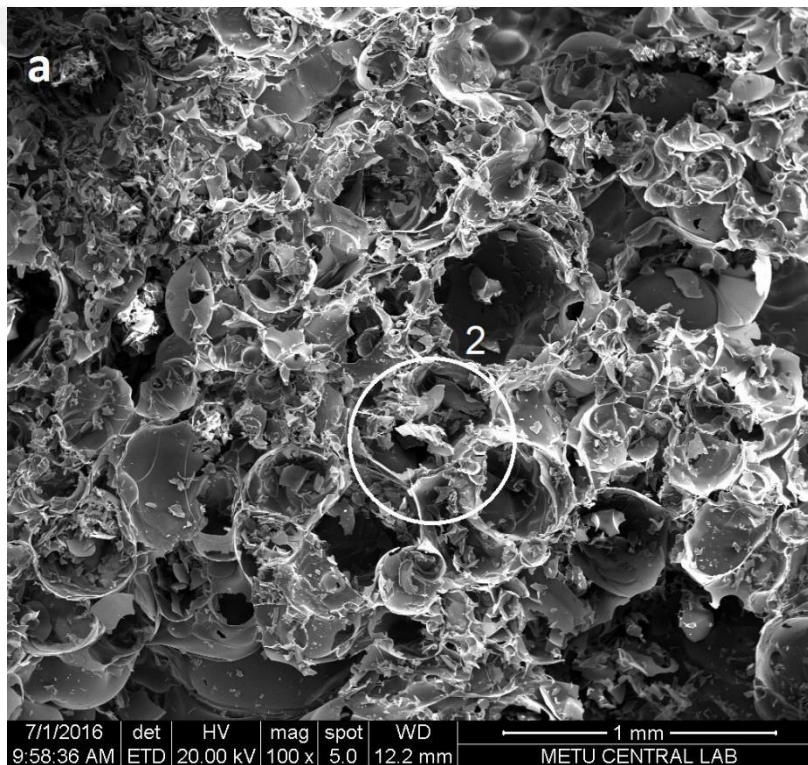| element	Si	O	Na	K
2 (wt.%)	33.50	40.98	20.03	0.68
3 (wt.%)	34.58	39.97	17.53	0.95

Figure 4.16 SEM images of sample made with the 16 M solution concentration: (a) 100× magnification, (b) 100× magnification from other point, (c) 500× magnification of (b), (d) 500×magnification of another point, (e) 2000× magnification of (d), (f) 50000× magnification of (e).
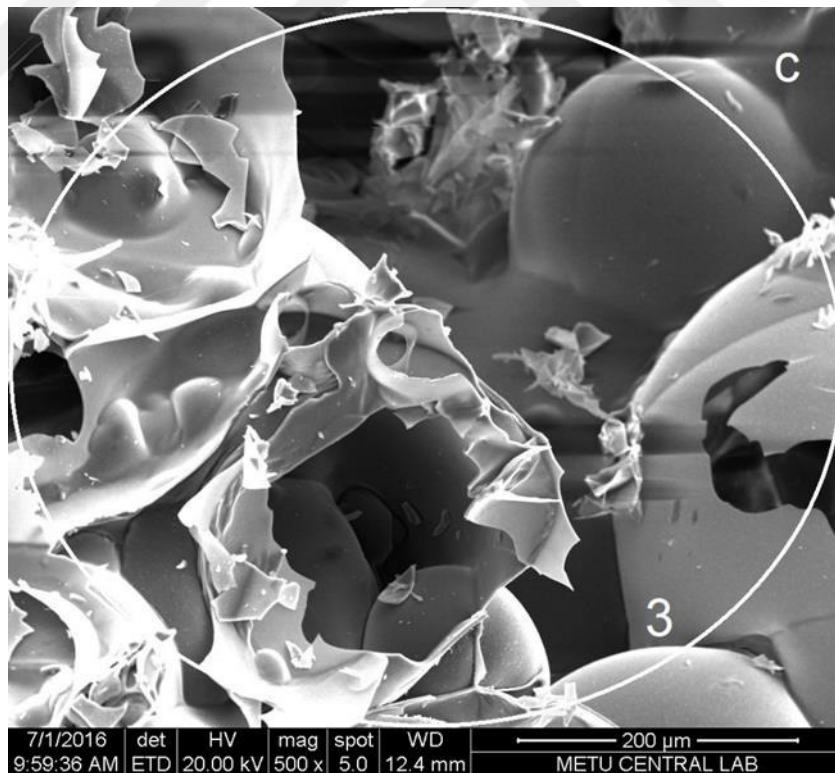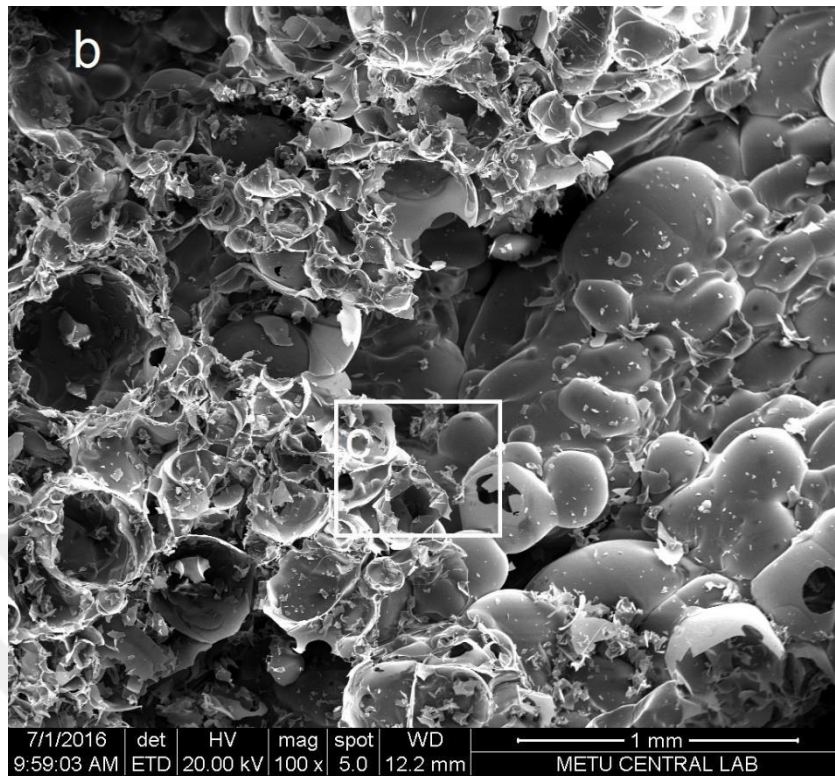
Figure 4.16 continued
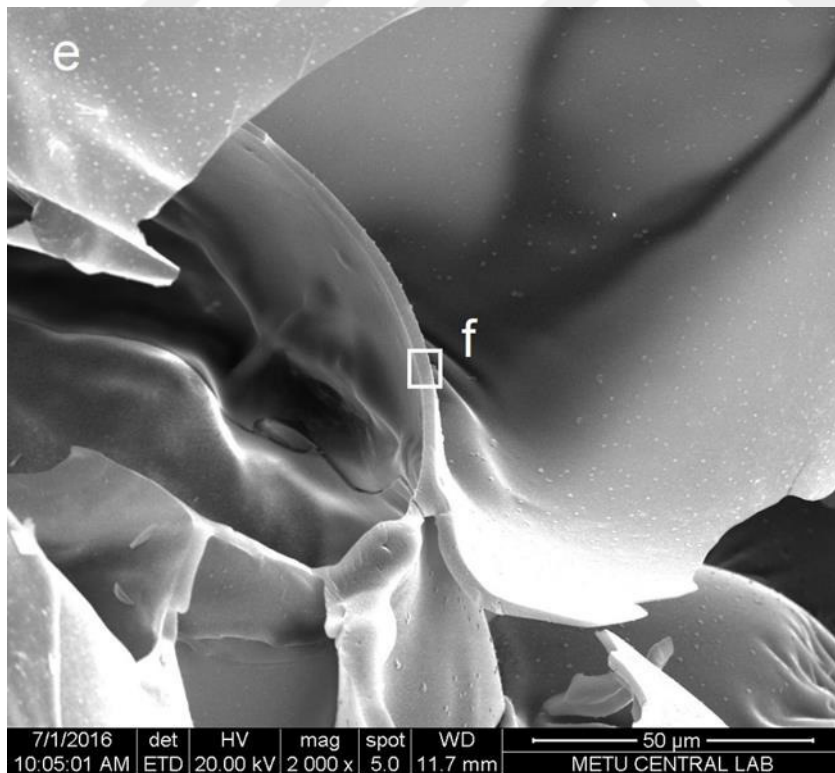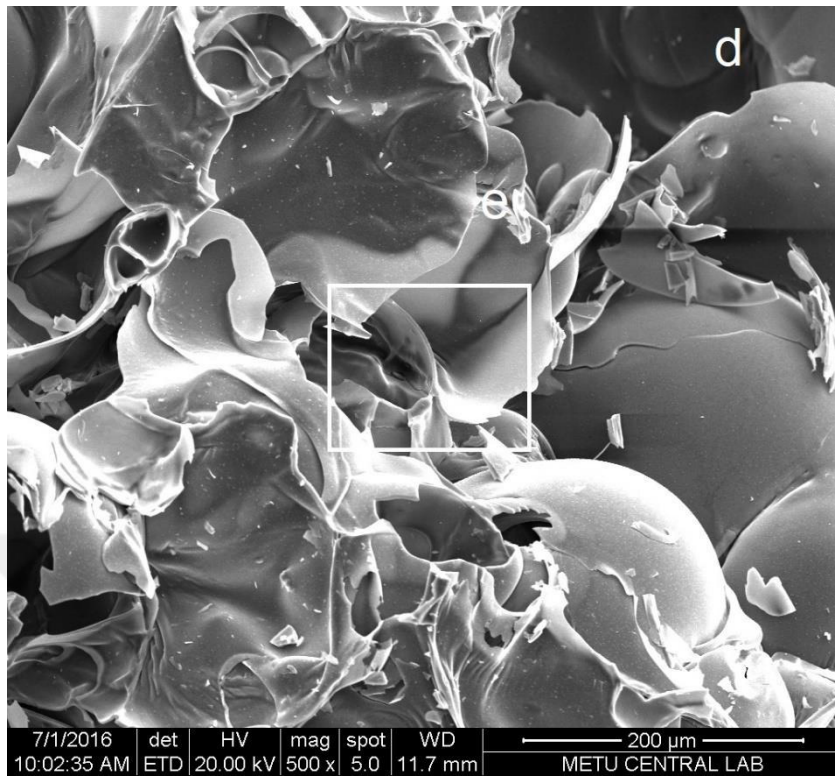
Figure 4.16 continued

Figure 4.16 continued

4.9.3 Sample made with 12M solution and A/P = 1

This was the most uniform sample detected visually. Figure 4.17 (a) shows a structure with fewer spherical pores but mostly what appears to be a collection of shards from what used to be hollow spheres. As the magnification increases it is observed that the pores are connected indicating potentially high permeability. The average thickness of septums in this concentrations range between 4 to 6 µm. EDX analysis of point 4 marked in 4.17 (d) is shown in Table 4.6. Na content and Si/O in between those of the 4 M and 16 M solutions activated samples is measured, as expected.

Table 4.6 Elemental composition for 12 M, A/P =1 from Fig 4.17 (d)

element	Si	O	Na	K
4 (wt.%)	35.06	41.83	17.89	0.44
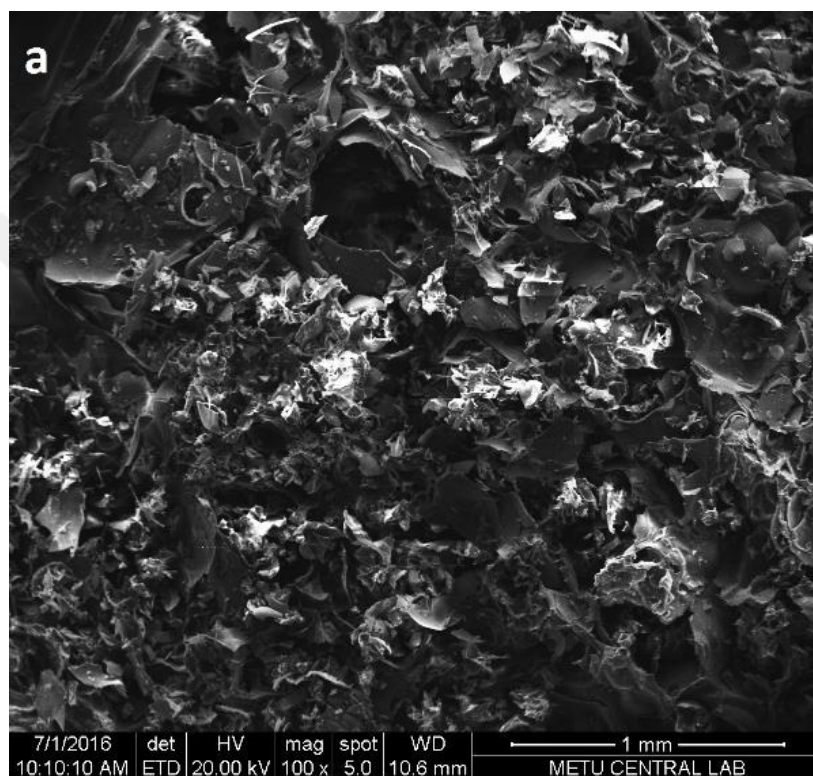
Figure 4.17 SEM images of 12 M samples (a) 100× magnification, (b) 200× magnification, (c) 500× magnification, (d) 2000× magnification.
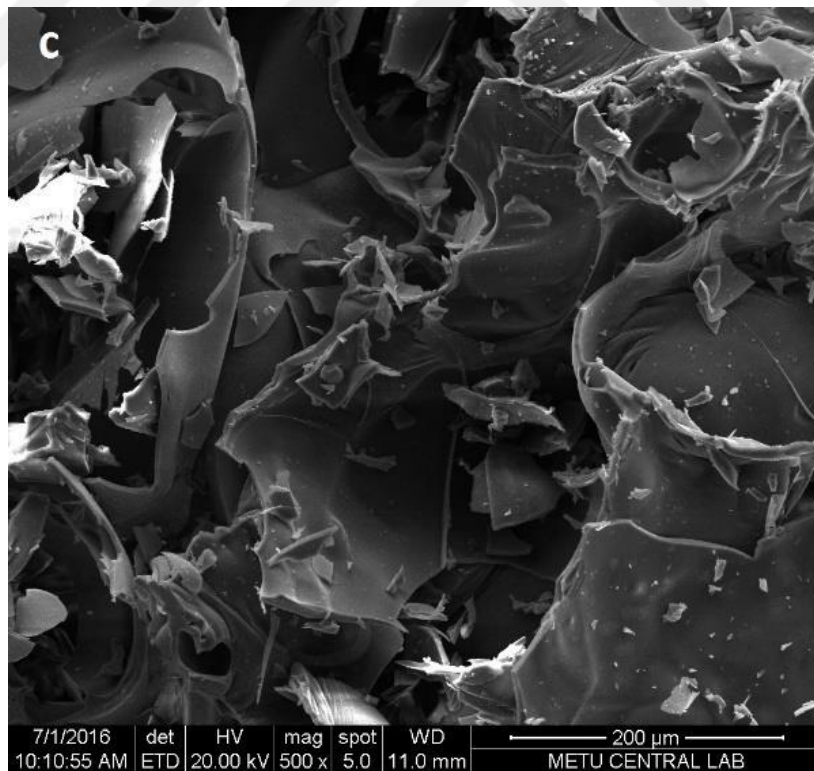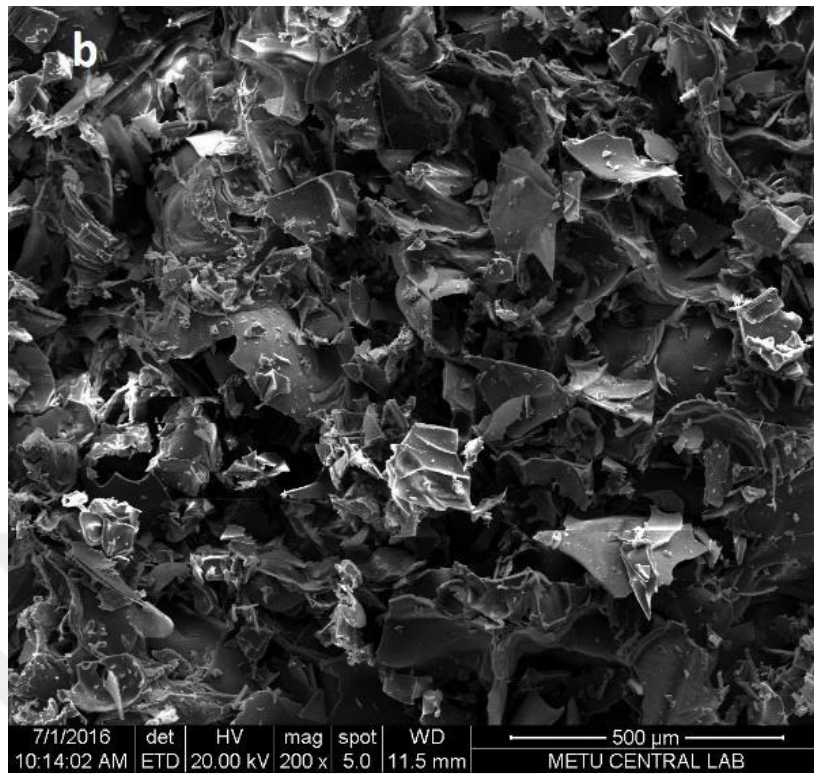
Figure 4.17 continued

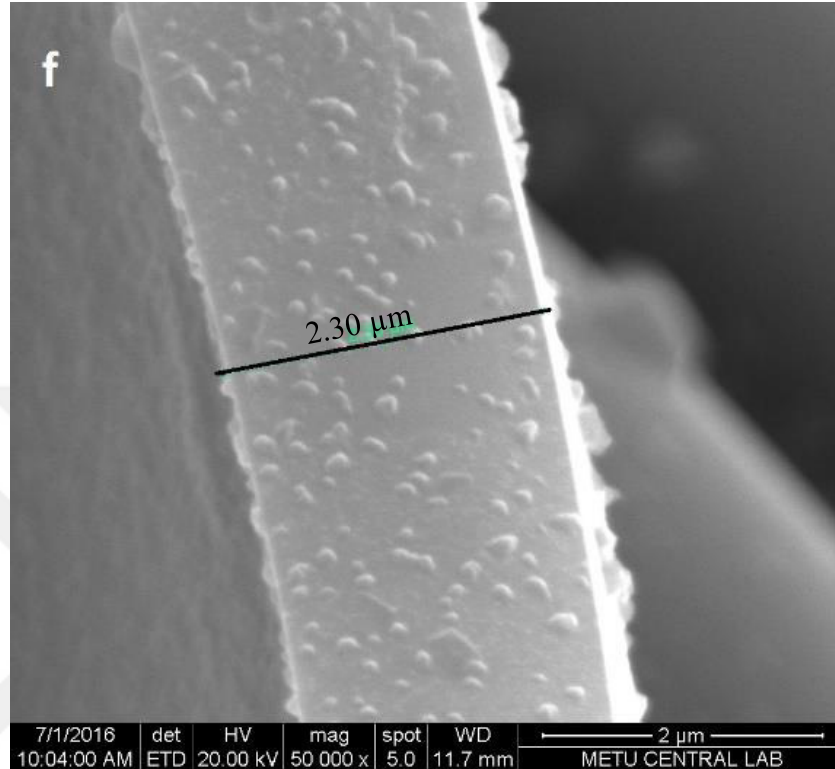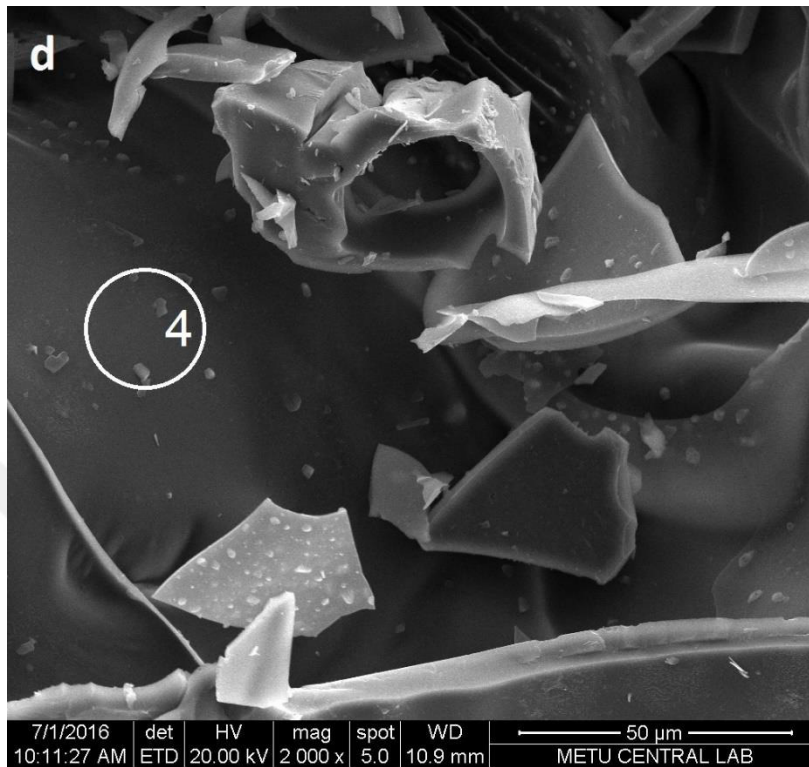*Figure 4.17 continued*

4.10 Compressive Strength

The final product obtained after curing and heat-treating the alkali-activated silica fume paste is a porous material with very low bulk specific weight and was not expected to possess high compressive strength. Most of the samples could even be compressed and broken by hand. Compressive loading was applied to the specimens to investigate their mechanical properties. Stress vs. strain response for four different samples made using different activating solution concentrations of is given in Figure 4.18.
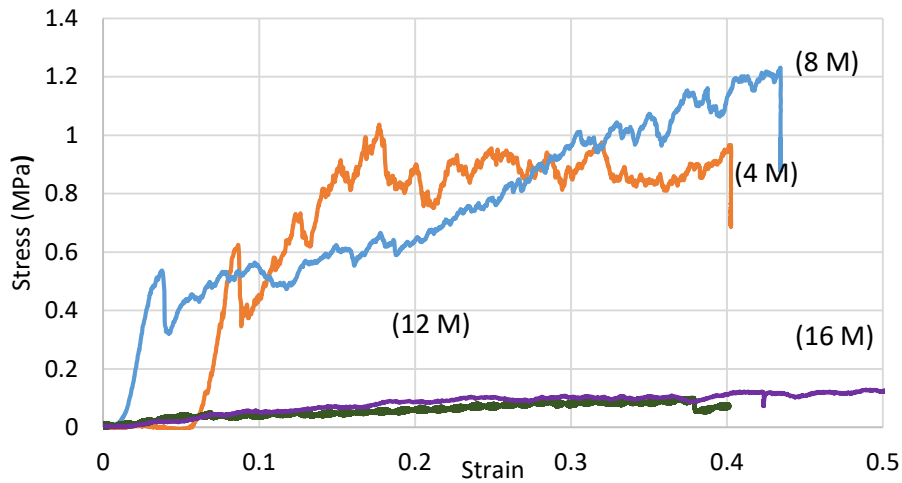
Figure 4.18 Stress vs. strain response of samples made using : (a) 4 M , (b) 8 M , (c) 12 M and (d)16 M NaOH activating solutions

Samples which were prepared with dilute NaOH solutions could withstand greater loads at the same deformation in comparison to those made with higher concentration solutions. These samples show different stages in resisting loads. They resist up to a specific load somewhat elastically and then compaction of the samples begins. The sample deforms somewhat during compaction of a (few) layers of pores after which the sample begins to resist the load once again and so on. In more concentrated activating solution mixtures, compressive strength is < 100 KPa, meaning they could not bear much load. For the purpose of improving the compressive strength of the samples, some additional materials were employed. Figure 4.19 gives the stress versus strain graph for these mixtures.
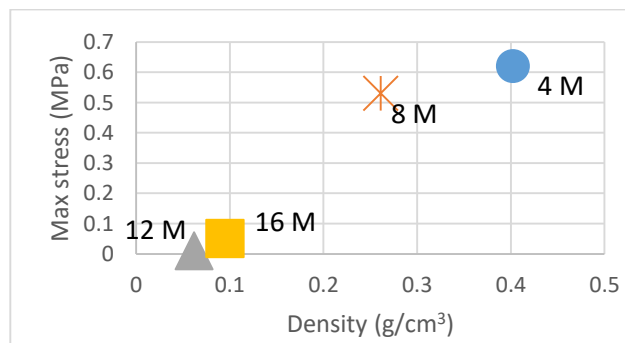
Figure 4.19 Maximum measured stress vs. bulk density for different expanded samples

63

Figure 4.19 shows that, as expected, strength and density of the expanded samples are roughly inversely related.
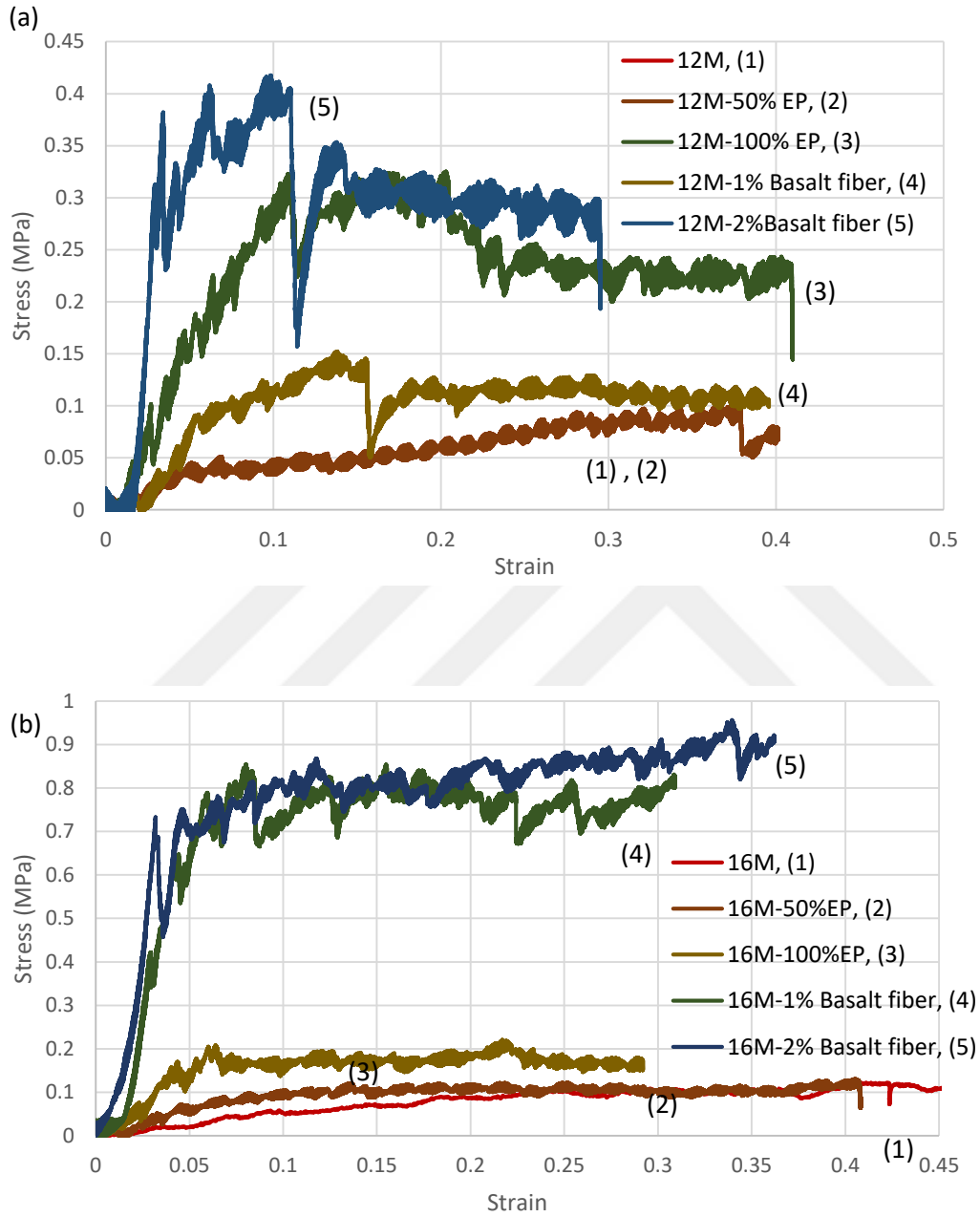
Figure 4.20 Stress vs. strain for samples made with (a) 12 M, (b) 16M activating solutions, using various additives

In both Figure 4.20 (a) and (b), the largest increase in compressive strength is observed when 2% basalt fiber was added to the mixture. Adding expanded perlite does not have much impact on the compressive strength of the 16M sample, but it increases compressive strength in 12 M samples up to 3 times.

4.11 Fourier Transform Infrared Spectroscopy Analysis

The progress of reactions and changes in the structure of bonds were evaluated using FTIR spectroscopy. Infrared spectra for the sample made using a 12 M NaOH solution in three different stages of preparation are shown in Figure 4.21.
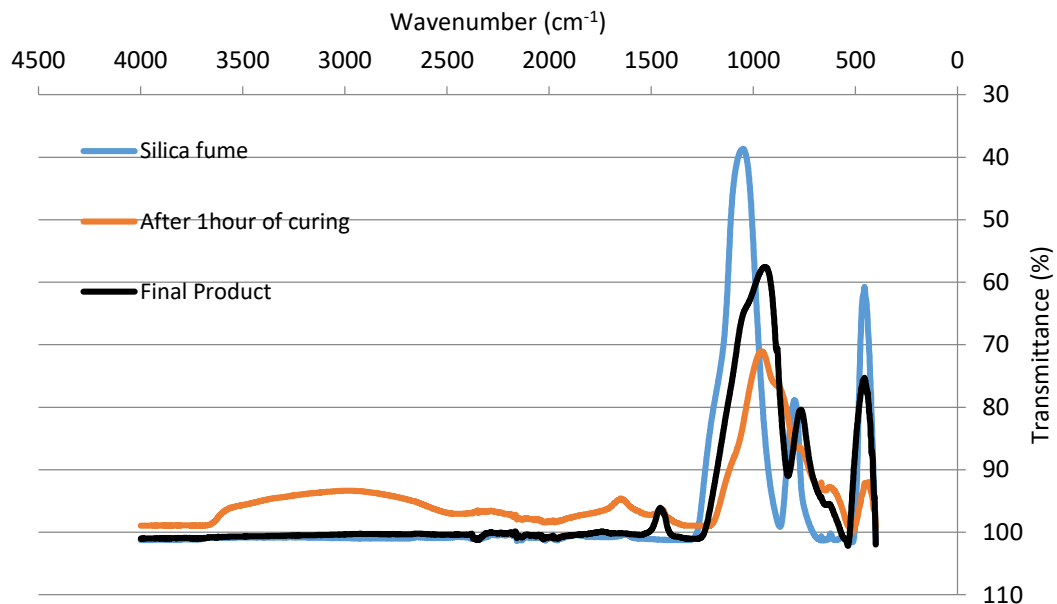
Figure 4.21 Infrared spectra for non-activated silica fume, activated SF paste after 1 h of curing, and 400 °C heat treated final product

It is obvious from Figure 4.21 that, the structures of silica fume and the final expanded product are more similar to each other than the sample cured for 1 hour at 100 °C. A high and sharp peak at 450 cm^{-1} in three stage of reaction, is assigned to the bending of Si–O bond in SiO$_4$ tetrahedron and it does not change its location during the process but the percentage of transmittance differs (Puertas et al., 2004). A very small peak at 620 cm^{-1} is detected in silica fume and during the reactions, this peak becomes stronger. This peak stands for the symmetric stretching of Si–O. The peak at 797 cm^{-}

[1] moves to 660 cm^{-1} and again in the final product comes back to 770 cm^{-1} wavenumbers. This peak belongs to the symmetric the stretching and vibrational Si–O band (Davidovits, 2008). The sharpest peak is located at 1050 cm^{-1} in silica fume and moves to a lower wavenumber during processing behavior typical in geopolymerazation. This peak corresponds to Si–O stretching assign to SiO_2 which is seen in quartz. This peak moves to the right during the preparation, and in the 1-hour cured sample, and final product peak decreases to 960 and 943 cm^{-1}, and these wavenumbers belong to stretching Si–O bond in Si–O–Na structure, respectively. This peak indicates gel type silicate or aluminosilicate formation.
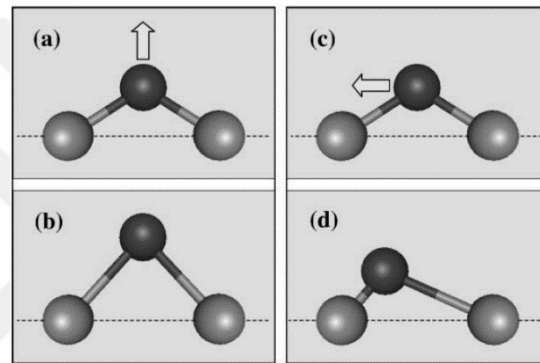
Figure 4.22 Motion of SiO$_2$ bonds; (a),(b) symmetric stretching, (c), and (d) asymmetric stretching parallel to Si-Si line (Innocenzi, 2003)

Figure 4.22 explains the symmetric and asymmetric Si-O stretching bonds. Oxygen atoms are shown with black and silicon atoms are shown with gray color in these oxygen bridging Si-O bonds. Terminal OH group and free water molecules are observed at different wave numbers. The small peaks at 1450, 1650, and 3000 cm^{-1} belong to these group of bonds in the 1-hour cured sample (Rovnaník et al., 2013). As expected, the peaks related to Si–OH form during curing where the NaOH attacks the silica fume particles breaking down their Si–O–Si structure. Then, upon polycondensation of two Si–OH (Si–OH + Si–OH → Si–O–Si + H_2O) the peaks related with Si–OH are lost again.

4.12 Nitrogen Adsorption

Various types, shapes, and sizes of pores exist inside the expanded material leading to the observed differences in volume and density of the final products. To investigate the pores inside the samples, nitrogen adsorption test was performed on three samples made with 8, 12 and 16 M sodium hydroxide solutions and A/P = 1. Samples were prepared in the optimum method was specified in Chapter 3.

Data of gas adsorption and desorption are presented in adsorption isotherms (Figure 4.23) which show the volume of adsorbed gas (V_a) with the change in the ratio of relative pressure (P/P_0).
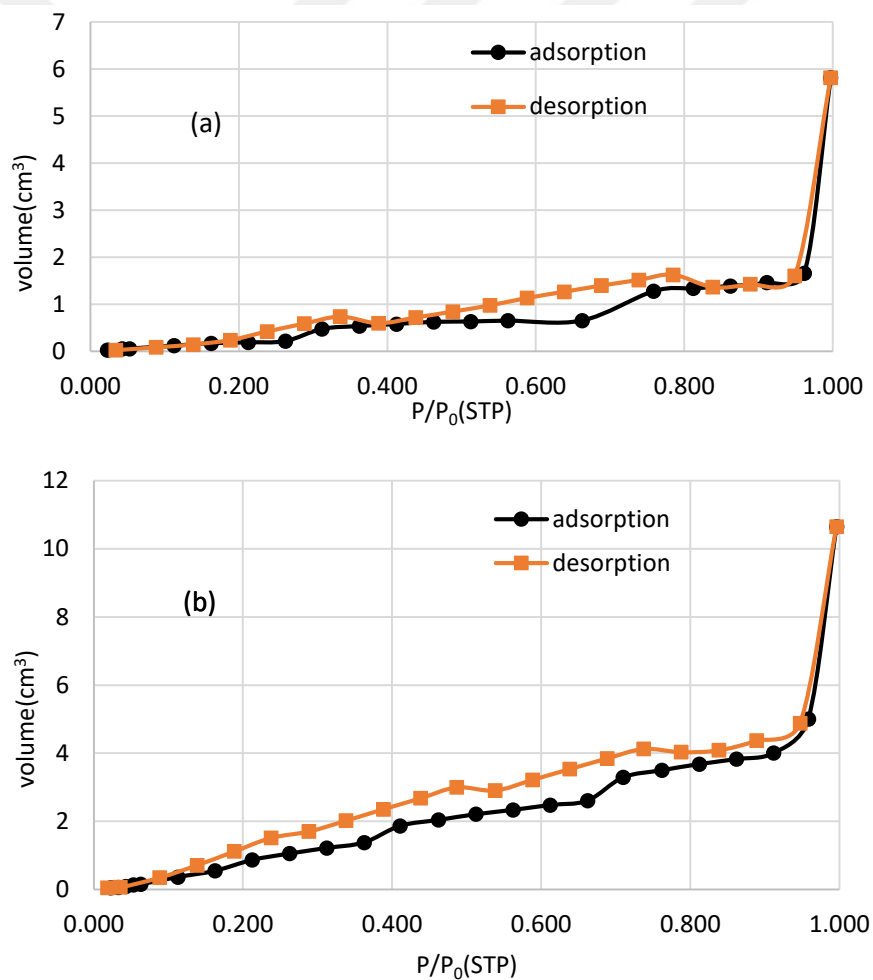
Figure 4.23 Adsorption isotherms of (a) 8 M, (b) 12 M and (c) 16 M concentration samples
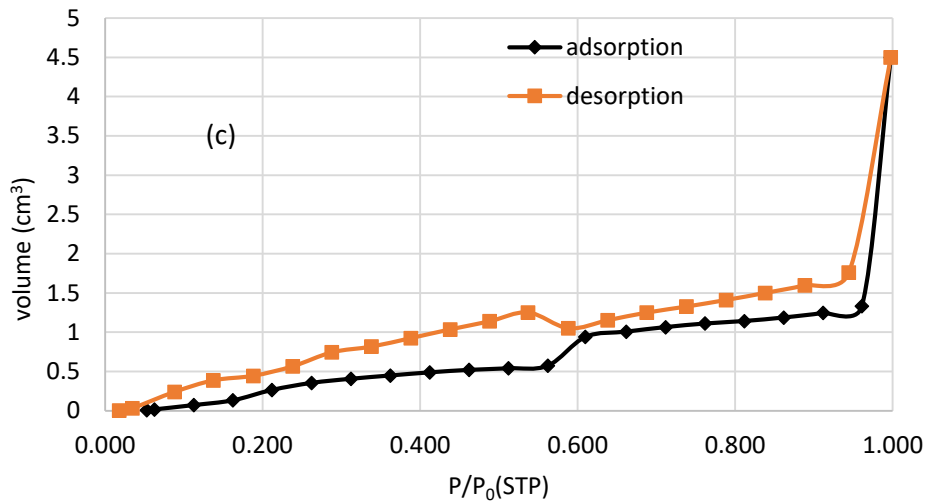
Figure 4.23 Continued

All samples have Type (V) adsorption (Rouquerol et al., 2013). This type of adsorption isotherm is recorded when the attraction between adsorbate molecules is higher than the interaction between adsorbate – adsorbent (N_2 and the sample surface). This also indicates that the material has microporous or mesoporous structure (Rouquerol et al., 2014). On the other hand, these graphs show capillary condensation during the test. Differences between the adsorption branch and the desorption branch form a hysteresis loop, indicating the presence of bottle-shaped pores inside the material. The shape of this loop is similar to H_4 hysteresis which indicates the presence of plate like pores inside the product (Sing, 1985). Extension of two adsorption desorption branch in lower pressures is because of swelling of the non-rigid porous structure or irreversible adsorption of adsorbate molecule in pores (Aligizaki, 2005; Sing, 1985).
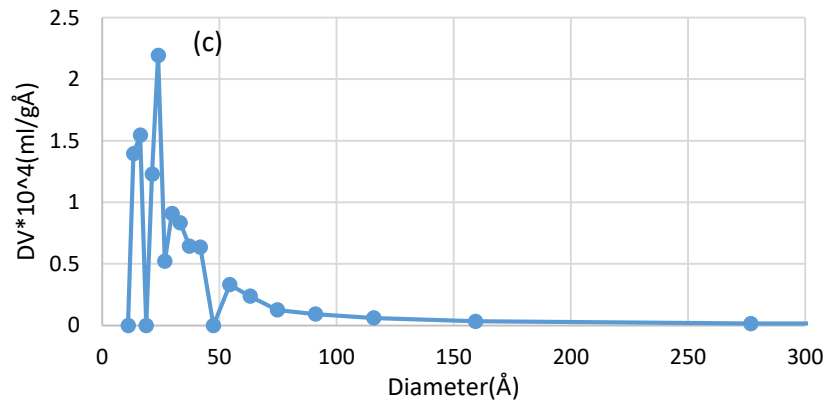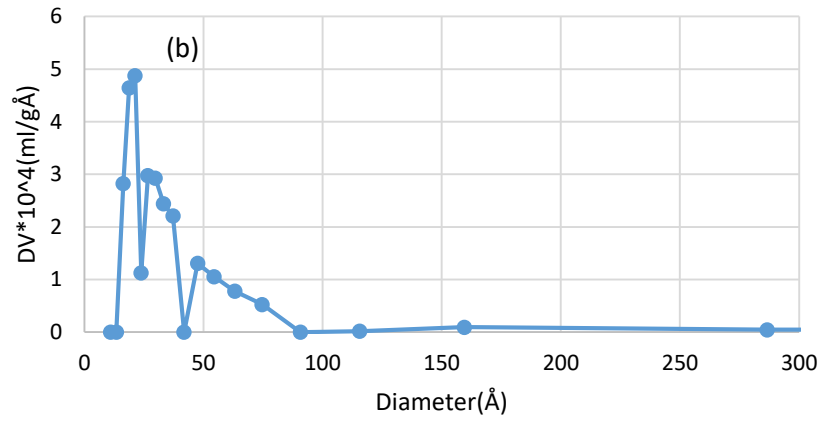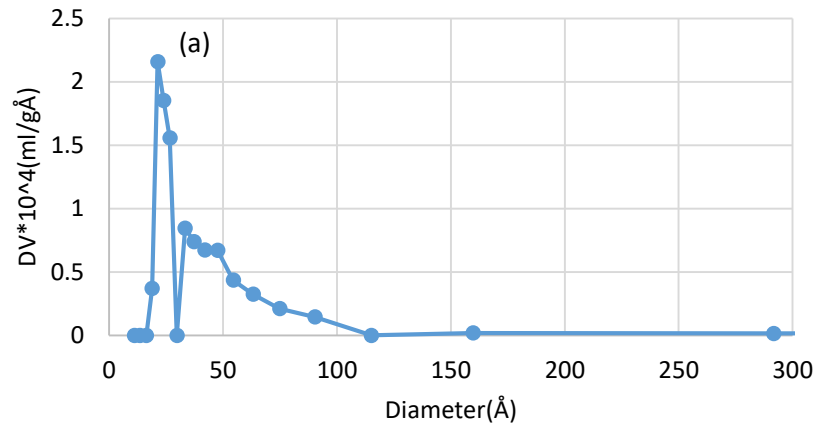
Figure 4.24 Pore size distributions of samples made using: (a) 8 M , (b) 12 M, (c) 16 M samples

The pore sizes of samples obtained from the desorption branch using Barrett-Joyner-Halenda (BJH) method and plotted as differential form of cumulative pore volume (DV) versus pore diameter for all the samples shows an abundance of pores around 10-30 Å (Figure 4.24). Considering pores with a diameter smaller than 20 Å as micropores and larger than 20 Å as mesopores, these samples can be categorized as the microporous. The greatest pore diameters among all these samples are observed in the 16M samples, measured as 4375 Å. The mode of pore diameter for each sample calculated using BJH desorption method is given in Table 4.7.

Table 4.7 Mode of pore diameter for different samples

Activating solution concentration (M)	4	8	16
Pore diameter (mode) (Å)	21.3	21.2	23.9

4.13 Micro Computed Tomography

A sample made with a 4 M activating solution, cured at 100 °C and heat treated at 300 °C, of dimensions 2.8×2.9×3.0 cm was scanned. The section images were taken approximately each 1 mm, and these images are used to simulate the 3-D volume of the sample shown in Figure 4.25.

As clearly observed in the Figure 4.25 the pores near the center of the sample join together, causing an increase in the pore size and local porosity.
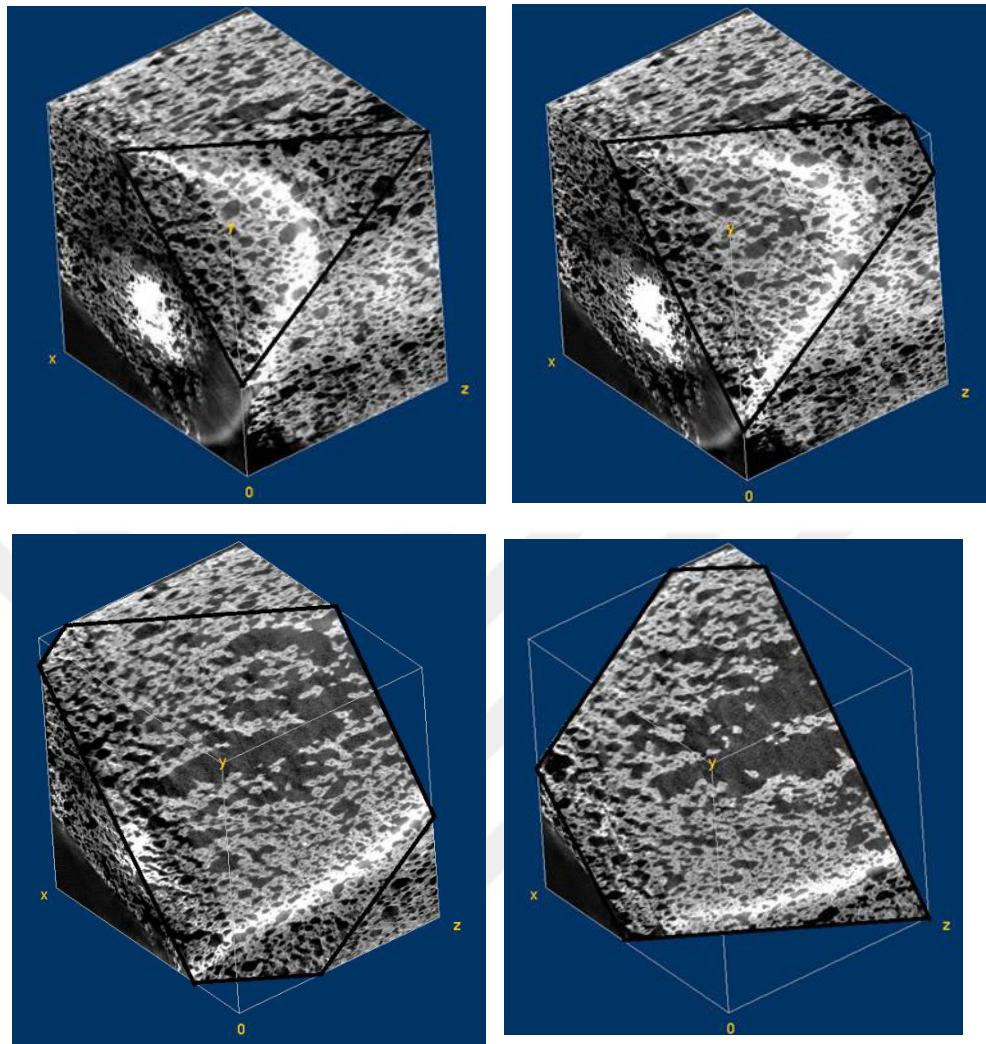
Figure 4.25 3-D volume simulation of 4 M solution (various cross-sections are shown)

Those changes in the porosity were calculated using Image J (an image processing software (Schneider et al., 2012)) and the result shows an increase from 34.2 % near the sides of the samples to 54.1 in the center of the sample. Because of limited access to the µCT scanner, the 12 M and 16 M solution samples could not be scanned. 12M samples were scanned using a flatbed scanner and presented in Figure 4.26. The result of porosity measurement shows approximately the same amount in both sections of the 12 M sample which proves the homogeneity of these samples assessed visually in earlier sections. The average porosity in these samples is about 45 - 50 %.
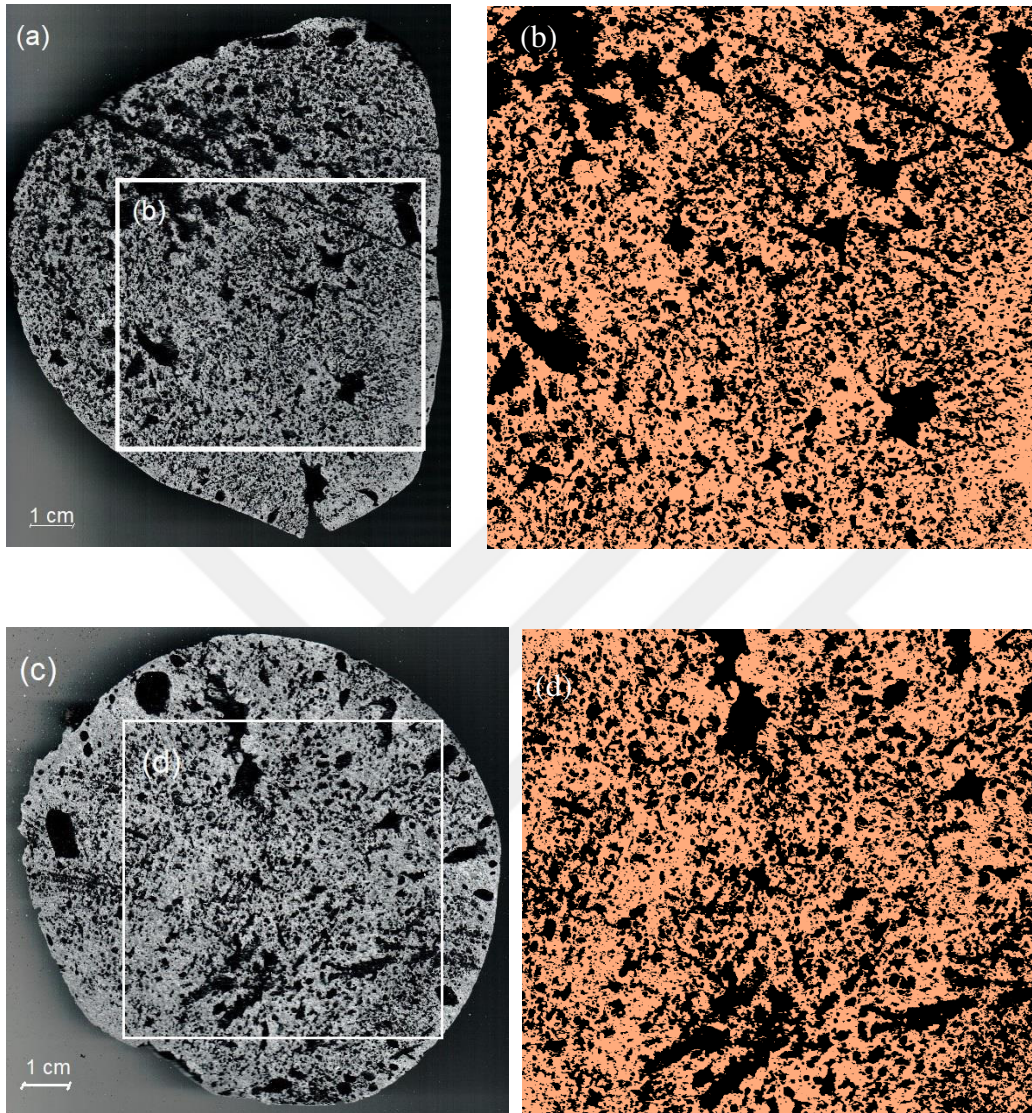
Figure 4.26 Flatbed scanned cross section of sample made using a 12 M activating solution: (a) near the surface, (b) porosity measurement using Image J near the surface,(c) flat scanned cross-section of center, (d) porosity measurement at the center of the sample.

4.14 NMR Analysis

Si NMR spectra of silica fume and NaOH-activated SF is provided Figure 4.27. Generally, the chemical shifts in silicates are in the range of -60 to -120 ppm. The chemical shifts revealed at -114 ppm with high intensity in silica fume is associated

with the presence of SiO$_2$ with the angles between 135 ° and 160 ° (Murdoch et al., 1985).
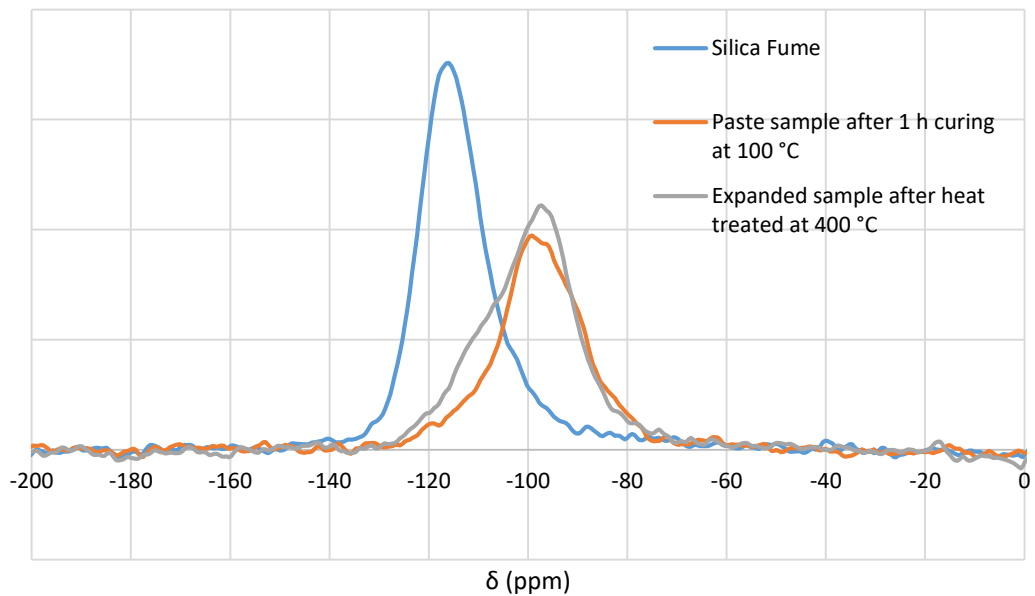
Figure 4.27 Chemical shift of 12 M solution sample from NMR results

This peak moves to -99.2 ppm in the 1-hour cured silica fume, which is related to the Q^3 tetrahedral units with the structural type of HOSi(OSi)$_3$ (Lippmaa et al., 1980; Maciel & Sindorf, 1980). Finally, the chemical shift is observed at -97.2 ppm which is attributed to the existence of condensed Q^3 tetrahedral units (Puertas et al., 2004; Rovnaník et al., 2013).

4.15 Water Absorption

The result of the water absorption test is given in Figure 4.28. In the first 48 hours the weight gain is similar in the two samples made using the solutions with different NaOH concentrations but afterwards, the rate of weight gain for 16 M samples passes that 12 M. Measurements should typically be continued until the increase in weight over a period over a period of 24 hours is less than 0.5 % of the greater weight, as specified in ASTM C 642. However, both samples dissolved in the water after some

time. The 12 M and 16 M samples could withstand being immersed in water for 7 days and 5 days respectively.
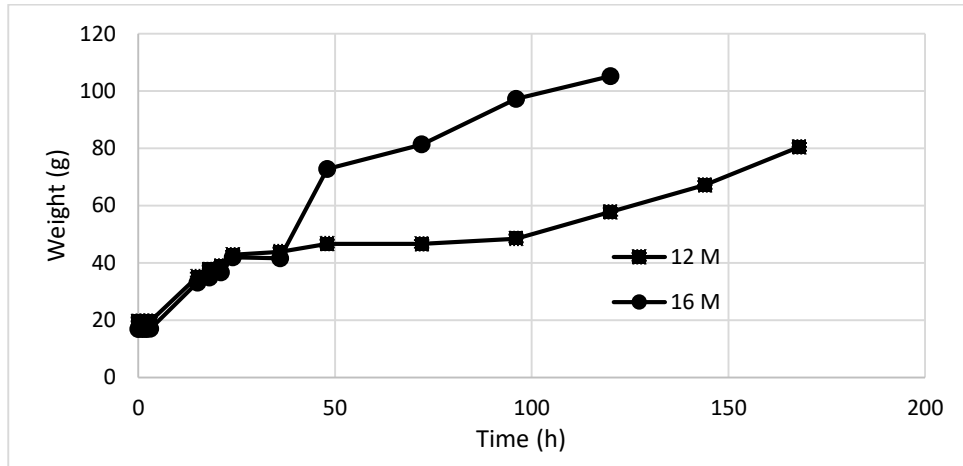
Figure 4.28 Weight measurement of 12 M and 16 M specimens during water absorption test

The percentage of water absorption for sample, calculated with Equation 3-1, is given in Table 4.8. The test shows that the 12 M samples can take water up to three times its initial weight and for the 16 M sample this value increases up to ~5 times of beginning weights.

Table 4.8 Percentage of water absorption

Sample Made with Solution Concentration (M)	12	16
Water Absorption (%)	312	525

CHAPTER 5

CONCLUSIONS

5.1 Concluding Remarks

In this thesis a low-value by-product material, the silica fume, was used to produce a thermally-insulating material. To reach this goal silica fume was activated with an economical alkali solution, NaOH. The activated SF paste was cured in oven and subsequently heat treated at high temperatures to expand it. Various tests were conducted and conclusions listed below were reached:

1. As the concentration of the activating NaOH solution used increases, the density of the final products decreases. Optimum density and homogeneity are reached with a 12 M NaOH.

2. 75 °C is the best mixing solution temperature to facilitate the mixing process.

3. Curing at 100 °C for 24 hours gave the best final expanded product. For heat treatment, approximately 4 hours (including the time to heat the oven and cooling) at a maximum temperature of 300 and 400 °C was found suitable.

4. Adding ground perlite did not improve in the products, but adding expanded perlite to the mixtures at an equal volume ratio (with the NaOH and SF mixtures) increased the compressive strength of products significantly.

5. Adding 2 wt. % of basalt fibers increases the compressive strength of products up to 1 MPa.

6. The highest compressive strength belonged to 4 M solution sample and the weakest to the 12 M concentrated ones.

7. Adsorption isotherms from nitrogen adsorption tests showed the presence of micropores and mesopores in the material which sometimes had ink bottle shapes. The hysteresis between adsorption and desorption isotherms indicated the existence of silt-shaped pores in the samples. During the nitrogen adsorption test, some swelling and irreversible adsorption took place.

8. Fourier transform infrared spectroscopy indicated the similarity of silica fume and the final expanded product, the existence of symmetric and asymmetric, normal and vibrational stretching Si-O bonds. The 1-hour cured sample was found to contain terminal OH bonds in the atomic structure of the material.

9. Scanning electron imaging indicated the foamy and porous nature of the expanded samples made with products in all concentrations. The pores are continuous and connected to each other. As the density decreases the porosity of samples increases more for the higher solution concentrations.

5.2   Recommendations for Future Studies

- Thermal conductivities of the expanded samples could be measured
- The use of other high silica can be investigated materials like diatomaceous earth or rice husk ash to achieve low density, porous materials.
- The use of other alkali solutions as (sodium silicate, KOH, etc.) can be investigated
- Silica fume can be mixed with other aluminosiliceous powders to achieve higher-strength and higher water resistance
- Viscosity modifiers could be used to achieve a mixture with a higher solution content and a lower powder content that still has viscosity suitable for setting and expansion so that even lower final densities can be achieved
- Small quantities of organic compounds such as epoxies could be added to the paste to improve properties like strength

REFERENCES

Abdullah, M. M. A. B., Jamaludin, L., Hussin, K., Bnhussain, M., Ghazali, C. M. R., & Ahmad, M. I. (2012). Fly ash porous material using geopolymerization process for high temperature exposure. *International Journal of Molecular Sciences*, *13*(4), 4388–4395.

Aït-Mokhtar, A., Hamami, A., Turcry, P., & Amiri, O. (2015). Porous Construction Materials: Characterizations and Modeling. In *Structure Design and Degradation Mechanisms in Coastal Environments* (pp. 1–39). John Wiley & Sons, Inc.

Aligizaki, K. K. (2005). *Pore structure of cement-based materials: testing, interpretation and requirements*. CRC Press, New York.

ASTM C642 (2013) Standard Test Method for Density, Absorption, and Voids in Hardened Concrete. ASTM International. West Conshohocken, PA.

Bapat, J. D. (2012). *Mineral admixtures in cement and concrete*. CRC Press, New York.

Bernal, S. A., & Provis, J. L. (2014). Durability of Alkali-Activated Materials: Progress and Perspectives. *Journal of the American Ceramic Society*, *97*(4), 997–1008.

Chandra, S., & Berntsson, L. (1996). 9 - Use of silica fume in concrete BT - Waste Materials Used in Concrete Manufacturing (pp. 554–623). Westwood, NJ: William Andrew Publishing.

Davidovits, J. (1994). Properties of geopolymer cements. In *First international conference on alkaline cements and concretes* (Vol. 1, pp. 131–149).

Davidovits, J. (2008). *Geopolymer chemistry and applications*. Geopolymer Institute, France.

Erdoğan, S. T. (2015). Inexpensive intumescent alkali-activated natural pozzolan pastes. *Journal of the European Ceramic Society*, *35*(9), 2663–2670.

Erdoğan, T. Y. (1997). *Admixtures for concrete*. Middle East Technical University

Press, Ankara.

EU Energy and Transport in Figures – Statistical Pocketbook, 2014.

Innocenzi, P. (2003). Infrared spectroscopy of sol–gel derived silica-based films: a spectra-microstructure overview. *Journal of Non-Crystalline Solids*, *316*(2), 309–319.

Ishizaki, K., Komarneni, S., & Nanko, M. (2013). *Porous Materials: Process technology and applications* (Vol. 4). Springer Science & Business Media, Tokyo.

Jaroniec, M., Kruk, M., & Olivier, J. P. (1999). Standard Nitrogen Adsorption Data for Characterization of Nanoporous Silicas. *Langmuir*, *15*(16), 5410–5413.

Limbachiya, M. C., & Kew, H. Y. (2008). *Excellence in Concrete Construction through Innovation: Proceedings of the conference held at the Kingston University, United Kingdom, 9 - 10 September 2008*. CRC Press, Leiden.

Lippmaa, E., Maegi, M., Samoson, A., Engelhardt, G., & Grimmer, A. R. (1980). Structural studies of silicates by solid-state high-resolution silicon-29 NMR. *Journal of the American Chemical Society*, *102*(15), 4889–4893.

Liu, P., & Chen, G. F. (2014). *Porous Materials: Processing and Applications*. Elsevier Science.

Mindess, S. (2014). *Developments in the Formulation and Reinforcement of Concrete*. Elsevier.

Neville, A. M., & Brooks, J. J. (1987). *Concrete Technology*. Longman Scientific & Technical, New York.

Olvianas, M., Najmina, M., Prihardana, B. S. L., Sutapa, F. A., Nurhayati, A., & Petrus, H. T. B. M. (2015). Study on the Geopolymerization of Geothermal Silica and Kaolinite. In *Advanced Materials Research* (Vol. 1112, pp. 528–532). Trans Tech Publ.

Paillere, A. M. (1994). *Application of Admixtures in Concrete*. Taylor & Francis, London.

Papadopoulos, A. M. (2005). State of the art in thermal insulation materials and aims for future developments. *Energy and Buildings*, *37*(1), 77–86.

Provis, J. L., & Bernal, S. A. (2014). Geopolymers and related alkali-activated

materials. *Annual Review of Materials Research*, *44*, 299–327.

Provis, J., & van Deventer, J. (2013). *Alkali Activated Materials: State-of-the-Art Report, RILEM TC 224-AAM*. Springer, Netherlands.

Prud'homme, E., Michaud, P., Joussein, E., Peyratout, C., Smith, A., Arrii-Clacens, S., Clacens J.M., Rossignol, S. (2010). Silica fume as porogent agent in geo-materials at low temperature. *Journal of the European Ceramic Society*, *30*(7), 1641–1648.

Prud'homme, E., Michaud, P., Joussein, E., Peyratout, C., Smith, A., & Rossignol, S. (2011). In situ inorganic foams prepared from various clays at low temperature. *Applied Clay Science*, *51*(1), 15–22.

Puertas, F., Fernández-Jiménez, A., & Blanco-Varela, M. T. (2004). Pore solution in alkali-activated slag cement pastes. Relation to the composition and structure of calcium silicate hydrate. *Cement and Concrete Research*, *34*(1), 139–148.

Ramamurthy, K., Kunhanandan Nambiar, E. K., & Indu Siva Ranjani, G. (2009). A classification of studies on properties of foam concrete. *Cement and Concrete Composites*, *31*(6), 388–396.

Rouquerol, F., Rouquerol, J., Sing, K. S. W., Maurin, G., & Llewellyn, P. (2014). 1 - Introduction BT - Adsorption by Powders and Porous Solids (Second Edition) (pp. 1–24). Oxford: Academic Press.

Rouquerol, J., Avnir, D., Fairbridge, C. W., Everett, D. H., Haynes, J. M., Pernicone, N., Ramsay, J. D. F., Sing, K. S. W., Unger, K. K. (1994). Recommendations for the characterization of porous solids (Technical Report). *Pure and Applied Chemistry*, *66*(8), 1739–1758.

Rouquerol, J., Rouquerol, F., Llewellyn, P., Maurin, G., & Sing, K. S. W. (2013). *Adsorption by powders and porous solids: principles, methodology and applications*. Academic press, Oxford.

Rovnaník, P., Bayer, P., & Rovnaníková, P. (2013). Characterization of alkali activated slag paste after exposure to high temperatures. *Construction and Building Materials*, *47*, 1479–1487.

Schneider, C. A., Rasband, W. S., Eliceiri, k. W. (2012) NIH Image to ImageJ: 25 years of image analysis. *Nature methods 9,671-675.*

Sadineni, S. B., Madala, S., & Boehm, R. F. (2011). Passive building energy savings: A review of building envelope components. *Renewable and Sustainable Energy Reviews*, *15*(8), 3617–3631.

Shi, C., Jiménez, A. F., & Palomo, A. (2011). New cements for the 21st century: The pursuit of an alternative to Portland cement. *Cement and Concrete Research*, *41*(7), 750–763.

Sing, K. S. W. (1985). Reporting physisorption data for gas/solid systems with special reference to the determination of surface area and porosity (Recommendations 1984). *Pure and Applied Chemistry*, *57*(4), 603–619.

Singh, B., Ishwarya, G., Gupta, M., & Bhattacharyya, S. K. (2015). Geopolymer concrete: a review of some recent developments. *Construction and Building Materials*, *85*, 78–90.

Soleimani Dorcheh, A., & Abbasi, M. H. (2008). Silica aerogel; synthesis, properties and characterization. *Journal of Materials Processing Technology*, *199*(1), 10–26.

Van Oss, H. G. (2014). *U.S. Geological Survey, Minera Commodity Summaries - Cement (pp. 38-39)*.

Vaou, V., & Panias, D. (2010). Thermal insulating foamy geopolymers from perlite. *Minerals Engineering*, *23*(14), 1146–1151.

Xu, R., Wu, C., & Xu, H. (2007). Particle size and zeta potential of carbon black in liquid media. *Carbon*, *45*(14), 2806–2809.

Zdravkov, B. D., Čermák, J. J., Šefara, M., & Janků, J. (2007). Pore classification in the characterization of porous materials: A perspective. *Central European Journal of Chemistry*, *5*(2), 385–395.